

Estimating black hole masses: Reverberation Mapping versus Accretion Disk Fitting

Samuele Campitiello^{1*}, Annalisa Celotti^{1,2,3}, Gabriele Ghisellini², and Tullia Sbarrato⁴

¹ SISSA, Via Bonomea 265, I-34135, Trieste, Italy

² INAF - Osservatorio Astronomico di Brera, via E. Bianchi 46, I-23807, Merate, Italy

³ INFN-Sezione di Trieste, via Valerio 2, I-34127 Trieste, Italy

⁴ Dipartimento di Fisica "G. Occhialini", Università di Milano - Bicocca, Piazza della Scienza 3, I-20126 Milano, Italy

Received ; accepted

ABSTRACT

We selected a sample of 55 Type 1 Active Galactic Nuclei with a black hole mass estimate inferred using the Reverberation Mapping technique and a clear evidence of the "Big Blue Bump" in the optical-UV band whose emission is produced by an accretion disk around a supermassive black hole. We fitted the spectrum of these sources with the relativistic thin accretion disk model KERRBB in order to infer the observed disk luminosity, the black hole mass and the Eddington ratio. The comparison between the masses inferred with the two methods led to the following results: 1] the two estimates are compatible within the uncertainties, assuming a black hole with a spin in the range $0 \leq a \leq 0.9982$ and a viewing angle of the system $\leq 45^\circ$; 2] the overall uncertainty on the black hole mass estimated through the disk fitting procedure is ~ 0.45 dex (which includes the uncertainty on the fitting parameters as the black hole spin and the viewing angle), comparable to the systematic uncertainty of Reverberation Mapping: however, such an uncertainty can be equal or smaller than ~ 2 if one of the parameters of the fit is well constrained; 3] although measurements are affected by large uncertainties, the comparison between the black hole masses inferred using the two methods led to a mean (logarithmic) value of the geometrical factor $\langle \text{Log } f \rangle = 0.63 \pm 0.49$ (at 1σ), consistent with previous estimates.

Key words. galaxies: active – (galaxies:) quasars: general – black hole physics – accretion, accretion disks

1. Introduction

Supermassive black holes (SMBHs) are located at the center of most galaxies and determining their mass and spin is crucial to understand their link with the host galaxy and the possible evolution in time.

Different methods have been used to have an estimate of the black hole (BH) mass: Reverberation Mapping (RM) technique (Blandford & McKee 1982; Peterson 1993; Netzer & Peterson 1997; Ho 1999; Wandel et al. 1999; Kaspi et al. 2000; Horne et al. 2004; Peterson et al. 2004; Bentz et al. 2009; see also the 2D velocity-delay maps Grier et al. 2013b), Single Epoch (SE) virial mass estimate (Vestergaard 2002; McLure & Jarvis 2002; McLure & Dunlop 2004; Wu et al. 2004; Greene & Ho 2005; Vestergaard & Peterson 2006; Kollmeier et al. 2006; Onken & Kollmeier 2008; Wang et al. 2009; Vestergaard & Osmer 2009; Greene et al. 2010; Rafiee & Hall 2011; Shen et al. 2011; Shen & Liu 2012; Trakhtenbrot & Netzer 2012), Accretion disk (AD) fitting (e.g., Malkan 1983; Sun & Malkan 1989; Wandel & Petrosian 1988; Laor 1990; Rokaki et al. 1992; Tripp et al. 1994; Ghisellini et al. 2010; Calderone et al. 2013; Campitiello et al. 2018, 2019, Microlensing in gravitationally lensed Quasars (QSOs) (e.g., Irwin et al. 1989; Lewis et al. 1998; Popovic et al. 2001; Richards et al. 2004; Morgan et al. 2010; Dai et al. 2010; Mosqueta & Kochanek 2011; Sluse et al. 2011; Guerras et al. 2013), Dynamical BH mass (e.g., Davies 2006; Onken et al. 2007; Hicks & Malkan 2008).

Each of them carries some uncertainties strongly linked to the features of the system and the parameters of the models involved for the measurements (Laor 1990; McLure & Jarvis 2002; Vestergaard & Peterson 2006; Marconi et al. 2008; Peterson 2010; Calderone et al. 2013), also enhanced by the quality of data. Therefore, it is necessary to improve these methods and set robust calibrations on the main scaling relations.

In this work, we chose to consider the RM technique because this method does not rely on scaling relations (e.g. like SE methods) and it is based on direct measurements related to the Broad Line Region (BLR), used to estimate the BH mass. This latter is expressed as:

$$M_{\text{BH}} = f \underbrace{\frac{c\tau_{\text{LT}} \sigma_{\text{line}}^2}{G}}_{=\text{VP}} \quad (1)$$

where f is the so-called geometrical factor (or virial coefficient) and VP is the virial product, function of the light-travel time τ_{LT} (i.e. the time related to the emission-line response delayed with respect to changes in the continuum) and the line velocity dispersion σ_{line} (see e.g., Ho 1999; Wandel et al. 1999)¹. The major uncertainty related to this estimate are carried by

¹ Some authors identify the virial product with the real BH mass, by considering the geometrical factor equal to ~ 1 (i.e. a spherical distribution of BLR clouds in randomly orientated orbits - Netzer 1990). Notice also that, the line velocity dispersion is often identified either as the line FWHM, or as the σ of the Gaussian profile used to fit the emission line.

* e-mail: sam.campitiello@gmail.com

the geometrical factor which depends on the geometry and orientation of the Broad Line Region (BLR, see Collin et al. 2006, Decarli et al. 2008): many authors have calibrated this factor comparing BH masses estimated from different methods (see Bentz & Katz 2015, and references therein). The RM technique estimates have a systematic uncertainty of $\sim 0.4 - 0.5$ dex (comparable to the SE one. Vestergaard & Osmer 2009), based on the comparisons between RM mass estimates and predictions from the $M - \sigma$ relation (e.g. Peterson 2010). Also the effect of the disk radiation pressure can affect the calibration of f , as the SE relations as well, especially for sources radiating close to Eddington (see Marconi et al. 2008; Netzer & Marziani 2010). For this reason, the comparison between different methods or the search of an alternative mean can help estimate BH masses in a more precise way.

The aim of this work is to compare two methods to estimate BH masses (RM and AD fitting) in order to understand the possible compatibility. We used Active Galactic Nuclei (AGNs) for which the black hole mass has been estimated from the RM technique. Among these sources, we selected the ones with a clear evidence of the so-called 'Big Blue Bump', in the rest-frame range $1000 - 5000 \text{ \AA}$, which is assumed to be produced by an AD around a central SMBH. We used the relativistic thin AD model KERRBB (Li et al. 2005) in order to estimate the observed disk luminosity, the Eddington ratio and the BH mass for different spin values:² in order to do so, an estimate of the spectrum peak position is necessary (see Campitiello et al. 2018 and Appendix B). It is important to notice that for very luminous QSOs the thin disk approximation breaks down because of the non-negligible disk vertical structure (the reference threshold is given by an Eddington ratio $\gtrsim 0.3$ - see Laor & Netzer 1989): the radiation pressure makes the disk inflate in the so-called "slim" or "thick" regime and other models must be used. One of these is SLIMBH (Abramowicz et al. 1988; Sadowski 2009; Sadowski et al. 2009; Sadowski et al. 2011)³ which accounts for relativistic effects and for the vertical structure of the disk, more appropriate for bright disks (see Koratkar & Blaes 1999); however, given its similarity with KERRBB, Campitiello et al. (2019) showed that, for a fixed spectrum peak, the differences in mass between the two models are less than a factor ~ 1.2 ; therefore, for the purpose of this work, we decided to use KERRBB, thought to be a good approximation of the AD emission.

The paper is structured as follows: in Sect. 2 we describe the AGN sample and the SED fitting procedure, also illustrating possible issues related to this approach (data uncertainties, absorption from dust, line contamination); in Sect. 3, we show the results (observed disk luminosity, BH mass and Eddington ratio) inferred from the different fits and compare them with the ones coming from the RM technique; Sect. 4 contains the final conclusions.

In this work, we adopt a flat cosmology with $H_0 = 68 \text{ km s}^{-1} \text{ Mpc}^{-1}$ and $\Omega_M = 0.3$, as found by Planck Collaboration XIII (2015).

2. Sample selection and fit procedure

In this section we describe the AGN sample and the SED fitting procedure we adopted to infer the observed disk luminosity, the Eddington ratio and the BH mass for each source, illustrating the possible issues related to this approach.

In order to select the sources of our sample, we used the AGN Black Hole Mass Database (Bentz & Katz 2015)⁴, a compilation of published spectroscopic RM studies of AGNs, the work of Lira et al. (2018), a RM study of high-redshift QSOs, the works of Grier et al. (2017, 2019) (Sloan Digital Sky Survey Reverberation Mapping Project) and the work of Hoorman et al. (2019) (AGN RM with the Australian Dark Energy Survey). We chose 55 sources (21 from the AGN Database, 9 from Lira et al. 2018, 4 from Grier et al. 2017, 19 from Grier et al. 2019, 2 from Hoorman et al. 2019), whose Spectral Energy Distribution (SED) shows a clear UV bump (the so-called "Big Blue Bump") produced by the radiation coming from the AD around the SMBH, resulting in an power law-like flux F_ν with a positive slope in the rest-frame wavelength range $3000 - 5000 \text{ \AA}$: this criterium enabled us to choose only sources with no contamination from the host galaxy whose emission, if very prominent, could interfere in the AD fitting procedure. Tables A.1 - A.2 list the sources of our sample along with the redshift, the BH mass estimates from the RM technique assuming a geometrical factor $f \sim 4$ (average value between the two extreme, most used/common values in literature, $f = 2.8 \pm 0.6$ and $f = 5.5 \pm 1.8$ - Onken et al. 2004; Graham et al. 2011, respectively), the line velocity dispersion, the light-travel time τ_{LT} , the SE BH mass estimates (using values from literature and relations from Shen et al. 2011 - see also Lira et al. 2018, Grier et al. 2017, 2019, Hoorman et al. 2019 for details), the observed disk luminosity L_d^{obs} , the BH mass M and the Eddington ratio λ_{Edd} (defined as the ratio between the total disk luminosity $L_d = \eta \dot{M} c^2$ and the Eddington luminosity $L_{Edd} = 1.26 \cdot 10^{38} M/M_\odot \text{ erg/s}$, where η is the disk radiative efficiency depending on the BH spin - see Appendix B for more details about these quantities)⁵ computed from the fit. The uncertainty on each quantity is described in the table caption.

2.1. Fitting procedure

For each source we found all the available photometric and spectroscopic data from literature and public archives (already corrected from Galactic extinction)⁶. We adopted the following fitting procedure:

- We fitted only the rest-frame spectrum ($\lambda - F_\lambda$, Fig. 1) with a power law to describe the AGN continuum, including the iron complex (Vestergaard & Wilkes 2001; Tsuzuki et al. 2006), some prominent emission lines (like MgII, CIII, CIV, SIV and Ly α) and a Balmer continuum (e.g., De Rosa et al. 2014), using GNU PLOT (non-linear least-squares Marquardt-Levenberg algorithm); after that, we performed another fit using the KERRBB model instead of the power law to describe the AGN continuum: the relativistic model overlaps well the power law for $\lambda > 1500 \text{ \AA}$ (the difference

⁴ See also <http://www.astro.gsu.edu/AGNmass/>.

⁵ As the total disk luminosity depends on the BH spin as well as the BH mass M (see Campitiello et al. 2018), also the Eddington ratio is a function of the spin as also shown in Figs. C.11 - C.20 in the Appendix.

⁶ The majority of the available spectra from public archives and literature is already corrected from Galactic extinction. When necessary, we performed this correction using the Cardelli et al. (1989) reddening law and E_{B-V} from Schlegel et al. (1998).

² The model is designed for stellar mass BHs and implemented in the interactive routing XSPEC; Campitiello et al. (2018) extended its usage also for SMBHs. Note that some issues about AD models for AGNs are still open (see e.g. Koratkar & Blaes 1999), also discussed in Campitiello et al. (2018).

³ As KERRBB, this model is implemented in XSPEC.

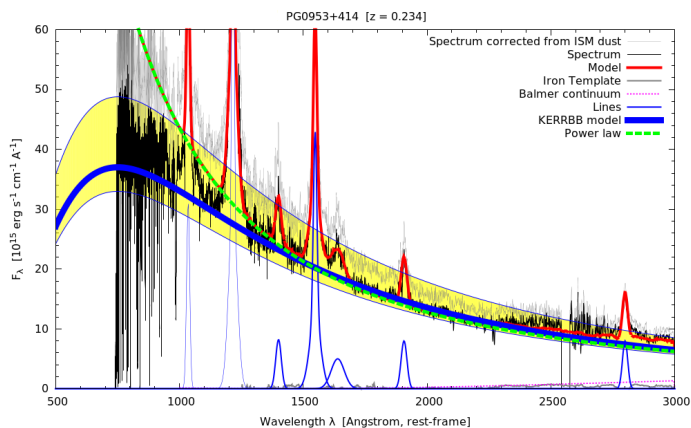


Fig. 1. Spectrum fit of the source PG0953+414 ($z = 0.234$) as a power-law continuum (dotted green line) plus the iron complex (gray line), the Balmer continuum (dotted purple line) and some prominent emission lines like MgII, CIII, CIV, SiIV and Ly α with a Gaussian profile (blue lines). The red line is the model of the spectrum given by the sum of all these components. The thick blue line is the KERRBB model of the continuum for which we defined a confidence interval (yellow area); the spectrum corrected from ISM dust (following the work of B16) is shown with a thin gray line (the confidence interval includes also the new fit performed after this correction). Notice that KERRBB overlaps well the power law for $\lambda > 1500$ Å: the difference at shorter wavelengths is due to the fact that the AD model is not a power law around the spectral peak.

at shorter wavelengths is due to the fact that the AD model is not a power law around the spectral peak - see the example in Fig. 1). For the majority of our sample, we used the curvature at wavelengths 2000 - 5000 Å in order to infer the spectrum peak frequency ν_p and luminosity νL_{ν_p} (once the viewing angle of the disk θ_v w.r.t. the line of sight is fixed, only these two quantities are necessary to infer the BH mass as a function of the spin - see Campitiello et al. 2018, 2019; see also Appendix B). When no spectroscopic data are present in this wavelength range, we estimated the peak position from the available spectrum at larger wavelengths.

- For each fit, we considered a confidence interval on the spectrum peak frequency and luminosity (± 0.05 dex on average - yellow area in Fig. 1 and blue area in Figs. C.1 - C.10) which corresponds to a confidence interval for the BH mass of about ± 0.1 dex on average.
- Although photometric data and their uncertainties are plotted along with the source spectrum, they are not taken into account in the fitting procedure because they might be contaminated by emission lines or by some kind of absorption (see below and also Figs. C.1 - C.10).
- The spectrum can be subjected to some absorption due to sky regions with a low transparency or, especially at high frequencies, to Lyman α clouds (for high redshift sources): even if the regions with a low sky transparency are subtracted from the spectrum, the best fit does not change and remains inside our confidence interval. For what concerns the spectral part absorbed by possible Lyman α clouds ($\text{Log } \nu \gtrsim 15.4$ Hz), the impossibility to have a reliable model to correct the spectrum at these wavelengths led us to exclude this spectral region from the fitting procedure.

An important effect that could modify the spectral UV shape concerns dust absorption that, if present, could lead to an incorrect BH mass estimate. The absorption could be caused by:

1. Dust in the host galaxy interstellar medium (ISM);
2. Dusty torus surrounding the AD.

Given that our sample is composed by Type 1 QSOs, we do not expect any absorption from the dusty torus, which is assumed to have an average opening angle of $\sim 45^\circ$: for this reason, in order to infer the BH mass, we assumed to observe each source with a viewing angle in the range $0^\circ \leq \theta_v \leq 45^\circ$ (see the Appendix for the results - BH mass and Eddington ratio - inferred in the cases with $\theta_v = 0^\circ - 30^\circ - 45^\circ$). However, we checked the goodness of our fit by considering the possible absorption by the host galaxy ISM: we followed the work done by Baron et al. (2016) (hereafter B16) who found an analytical expression to infer the amount of absorption (in terms of E_{B-V}) as a function of the observed spectrum slope α_v in the wavelength range 3000 - 5100 Å.⁷ In order to correct the spectrum from dust, we performed the following procedure:

- For each source, we found the index α_v of the power law (describing the AGN continuum), that can also be expressed using Eq. (1) in B16, and computed the extinction E_{B-V} following B16 (we reported the value related to each source in Table A.1 - A.2).
- Then, we corrected the UV spectrum using the extinction law described by Czerny et al. (2004) and fitted the new one with KERRBB.

The results of this procedure are reported in Tables A.1 - A.2: for the majority of the sample, the correction is small and the results are inside the confidence interval already defined without the correction from dust; for 4 sources, we reported the results of the new fit. Note that we did not apply this procedure for some sources because no spectroscopic data are available in the considered wavelength range for the evaluation of α_v .

Moreover, for a more complete analysis on the possible UV dust absorption, for each source we also performed the following procedure: we used the extinction law of Czerny et al. (2004) and assumed that the slope of the corrected, de-reddened spectrum at wavelength < 2000 Å had to be softer than the theoretical value $F_\nu \propto \nu^{1/3}$. In this way, we found an upper limit for the correction (on average $E_{B-V} \sim 0.25$) that led to a decrease of the BH mass obtained through the SED fitting procedure at most by a factor of ~ 0.3 dex (since the spectrum peak position changes due to the correction). As explained before, since we are dealing with Type 1 QSOs, we do not expect such a strong UV absorption. Therefore, for our analysis, we decided to consider only the (on average, small) correction E_{B-V} inferred following B16 in order to compute the BH mass.

In the next section, we show the results coming from the SED fitting procedure. We used the analytical expressions found by Campitiello et al. (2018) (see also Appendix B) in order to infer the observed disk luminosity, the BH mass and the Eddington ratio (reported in Tables A.1 - A.2), in the spin range $0 \leq a \leq 0.9982$ and viewing angles $0^\circ \leq \theta_v \leq 45^\circ$: following the authors, all these solutions describe the same spectrum with the same peak position: in fact, assume that a spectrum can be described for some values of the parameters M , \dot{M} and a ; by changing these parameters appropriately, it is possible to reproduce the same original spectrum.

⁷ Note that possible deviations from the average continuum slope could be caused by other factors connected to the BH physics, such as the BH mass, the accretion rate, the spin and the system orientation (Hubeny et al. 2000; Davis & Laor 2011).

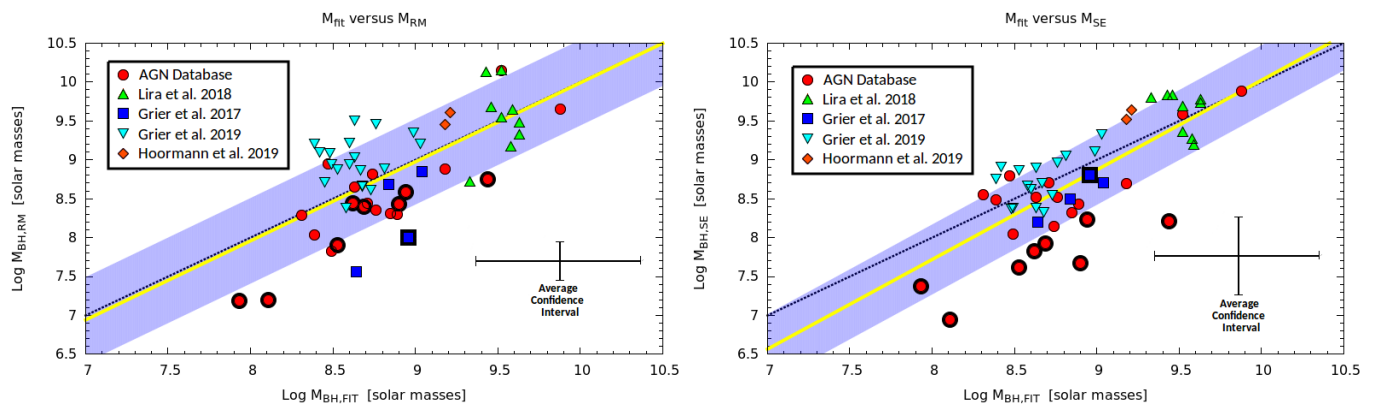


Fig. 2. Left panel: comparison between the BH mass estimates from the SED fitting procedure and the BH masses calculated from RM with a fixed factor $f \sim 4$ (average value between 2.8 ± 0.6 and 5.5 ± 1.8 - reference values from Graham et al. 2011 and Onken et al. 2004, respectively). For the average uncertainties, see text and Tables A.1 - A.2). The thick yellow line is the best fit ($\text{Log } M_{\text{BH, RM}} \propto 1.02 \text{ Log } M_{\text{BH, FIT}}$) and the shaded area is the 1σ dispersion of data (~ 0.55 dex) around the best fit line. This plot does not change significantly if we use the same factor f as reported in each work we referred to ($f = 4.3$ for the AGN database sources, $f = 1$ for Lira et al. 2018, $f = 4.47$ for Grier et al. 2017, 2019, $f = 1$ for Hoorman et al. 2019). Right panel: same comparison with the SE BH mass estimates. The uncertainty on the SE estimates is ~ 0.5 dex (e.g. Vestergaard & Osmer 2009). The thick yellow line is the best fit ($\text{Log } M_{\text{BH, RM}} \propto 1.15 \text{ Log } M_{\text{BH, FIT}}$) and the shaded area is the 1σ dispersion of data (~ 0.45 dex). In both plots: the dotted black line is the equality line. Points with a thick black contour correspond to the sources of our sample for which a large extinction $E_{B-V} (\gtrsim 0.07)$ has been adopted in order to correct the spectrum from ISM dust, following the work of B16 (see Appendix A and group [D] in Tab. A.1).

3. Results

In this Section we show the BH mass coming from the SED fitting procedure and compare it to the one obtained through the RM technique.

3.1. BH Mass comparison

The left panel of Fig. 2 shows the comparison between the BH mass from the SED fitting procedure and the BH mass from RM⁸ (see Tables A.1 - A.2 and Figs. C.11 - C.20 for results and details). The uncertainty on the BH mass from the fit is ~ 0.45 dex (comparable to the systematic uncertainties on the RM and SE estimates); this uncertainty is connected to different quantities involved in the fitting procedure:

1. BH Spin, in the range $0 \leq a \leq 0.9982$;
2. Viewing angle of the AD w.r.t. our line of sight, in the range $0^\circ \leq \theta_v \leq 45^\circ$;
3. Uncertainty on the spectral peak frequency ν_p and luminosity $\nu_p L_{\nu_p}$.⁹

The uncertainty on the RM BH mass is given by the uncertainty on the light-travel time and the line velocity dispersion

⁸ Each dot related to the BH mass from the fitting procedure corresponds to the mean BH mass computed using the extreme values given by the uncertainties. Instead, each dot related to RM corresponds to a BH mass with a fixed geometrical factor $f \sim 4$: these BH masses are originally estimated using different values of f , from 2.8 ± 0.6 to 5.5 ± 1.8 (Graham et al. 2011 and Onken et al. 2004, respectively); we have recalculated them assuming the same value of f , for all sources.

⁹ The BH mass changes by ~ 0.5 dex going from $a = 0$ to $a = 0.9982$, and by ~ 0.2 dex going from $\theta_v = 0^\circ$ to $\theta_v = 45^\circ$ for a fixed spin (assuming that the AD emission is not obscured completely by the dusty torus with an average opening angle of $\sim 45^\circ$): taking as a reference value the arithmetic mean of the BH mass in the whole spin range (as done in this work), the overall uncertainty is ~ 0.35 dex. Moreover, by considering also the uncertainty on the spectral peak position (on average ~ 0.05 dex), the BH mass has an additional uncertainty of ~ 0.1 dex on average.

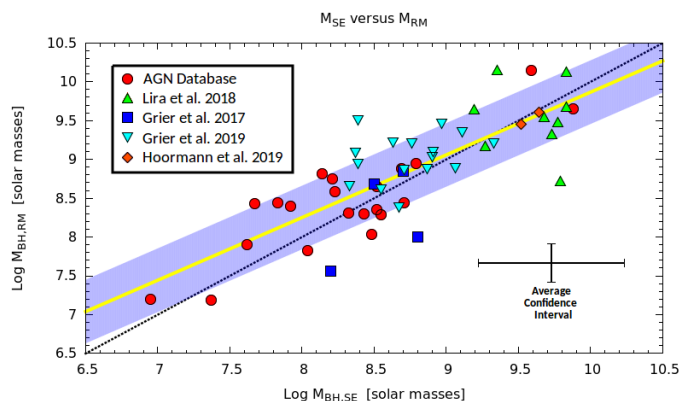


Fig. 3. Comparison between the SE BH mass estimates and the corresponding RM BH mass estimates with the same factor $f \sim 4$. The 1σ dispersion of data is ~ 0.4 dex around the best fit line ($\text{Log } M_{\text{BH, RM}} \propto 0.81 \text{ Log } M_{\text{BH, FIT}}$). The dotted black line is the equality line. (see text and Tables A.1 - A.2 for details about the average uncertainties).

(as reported in the AGN database and the RM reference papers) and by the mass interval obtained by assuming $(2.8 \pm 0.6) < f < (5.5 \pm 1.8)$ (the RM systematic uncertainty is $\sim 0.4-0.5$ dex - Peterson 2010). Notice that if the spectral peak is well constrained (and/or the viewing angle of the system is known), the mean uncertainty on the AD BH mass estimates can be of a factor of ~ 2 or even smaller.

Although the dispersion is not small, the best fit line (yellow line, $\text{Log } M_{\text{BH, RM}} \propto 1.02 \text{ Log } M_{\text{BH, FIT}}$, with a correlation coefficient $r \sim 0.67$) is consistent with the 1:1 line (dotted black line) with a 1σ dispersion of ~ 0.55 dex.

Figure 2 (right panel) shows the comparison between the BH mass from the SED fitting procedure and the BH mass from SE relations (as reported in the corresponding papers). The uncertainty on the SE estimates is ~ 0.5 dex similar to the systematic

one of RM (e.g. Vestergaard & Osmer 2009). The best fit line is $\text{Log } M_{\text{BH, RM}} \propto 1.15 \text{ Log } M_{\text{BH, FIT}}$ (with a correlation coefficient $r \sim 0.75$) consistent with the 1:1 line within the uncertainties, with a 1σ dispersion of ~ 0.4 dex, less than the one in the left panel of Fig. 2. We want to stress that, even if RM results are in good agreement with the SE ones (Fig. 3), given the large systematic uncertainties on both estimates, the small dispersion related to SE results cannot be ascribed to a better compatibility of such estimates with the ones coming from the fitting procedure.

In both panels of Fig. 3, 9 points have been marked with a thick black contour, corresponding to sources for which a large extinction $E_{B-V} (\gtrsim 0.07)$ has been adopted in order to correct the spectrum from ISM dust, following B16 (see Appendix A and group [D] of Tab. A.1). In the right plot, these sources are incompatible with the 1:1 line by a factor larger than $\sim 3 - 4$ (corresponding to $\sim 2 - 3\sigma$); the explanation could be related to the possible (strong) absorption of the UV emission by dust: SE relations are in the form $\text{Log } M = a + b \text{ Log } L_\nu + 2 \text{ Log FWHM}$, where a and b are positive coefficient calibrated using BH mass estimates coming from different methods, and L_ν is the continuum luminosity at a particular frequency; if the continuum luminosity and the line FWHM are underestimated due to a possible dust absorption of the UV emission, the resulting BH mass will be smaller. Therefore, the correction of the UV emission from dust absorption leads to a larger SE BH mass and a smaller BH mass from the SED fitting procedure (since the spectral peak frequency shifts to larger values - see Eq. B.4), making the marked points in Fig. 2 shift towards the blue shaded area.¹⁰

In the next Section, we describe the geometrical factor f distribution, given by the comparison between the BH masses estimated from the fitting procedure and RM ones.

3.2. Distribution of the factor f

The value of the geometrical factor f spans a large range of values with a significant scattering (e.g. Graham et al. 2011; Onken et al. 2004) mostly due to our ignorance on the BLR geometry and to the systematic uncertainties involved in the measurements. Using our sample, in this Section, we want to study the distribution of the geometrical factor f starting from the assumption that the BH mass $M_{\text{BH, FIT}}$ estimated from the AD fitting procedure is the real BH mass; this choice relies on the fact that the model KERRBB does not depend on the geometry of the BLR and it is an independent method to estimate the BH mass without taking into account distances and velocities (as the RM technique does).

Hence, by combining the AD fitting results with RM, the BH mass can be written as

$$M_{\text{BH, FIT}} = f \text{ VP}, \quad (2)$$

where the virial product VP is computed using the data reported in Tables A.1 - A.2. Then we calculated the ratio $M_{\text{BH, fit}}/\text{VP}$ in order to find the value of f (Fig. 4, top panel). The mean (logarithmic) value is $\langle \text{Log } f \rangle = 0.63 \pm 0.49$ at 1σ , which is consistent within the uncertainties with the most used/common values $\langle f \rangle = 2.8 \pm 0.6$ (Graham et al. 2011), $\langle f \rangle = 4.3 \pm 1.1$ (Grier et al. 2013a), $\langle f \rangle = 4.47^{+1.42}_{-1.08}$ (Woo et al. 2015), $\langle f \rangle = 5.5 \pm 1.8$ (Onken et al. 2004). Notice that, this result is based on the fact that we are considering the whole BH spin range $0 \leq a \leq$

¹⁰ Using $b = 0.5$ (calibration from Vestergaard & Peterson (2006) related to the H β line, a modification of 0.2 dex in the continuum luminosity, and a modification of a factor 1.25 of the FWHM correspond to a modification of the BH mass of ~ 0.1 and ~ 0.2 dex, respectively.

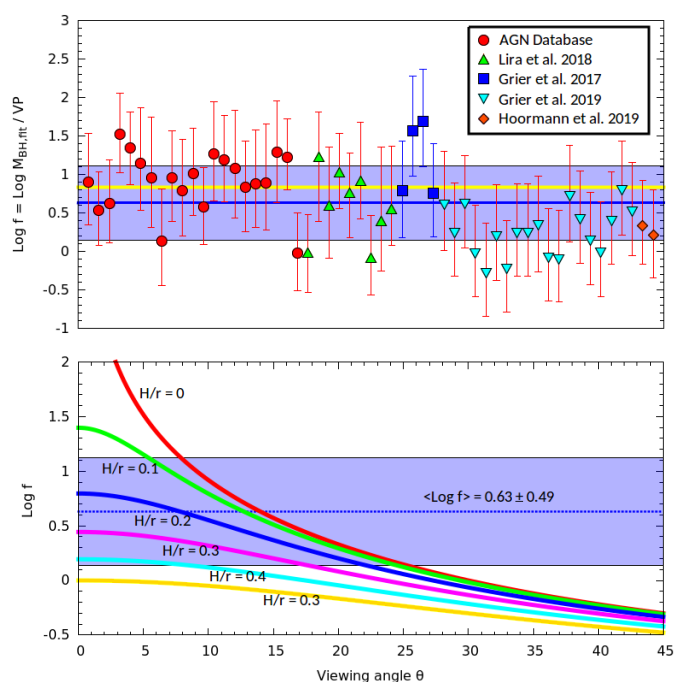


Fig. 4. Top panel: distribution of the factor f given by the ratio between the BH mass obtained through the SED fitting procedure and the VP (Eq. 2) (see text for the average uncertainties and Tables A.1 - A.2). The mean (logarithmic) value is $\langle \text{Log } f \rangle = 0.63 \pm 0.49$ at 1σ , consistent with previous estimates; notice that this result is based on the fact that we are considering the whole BH spin range $0 \leq a \leq 0.9982$: if we assume that the BH spin is equal to the maximum allowed value ($a = 0.9982$), then we mean value is $\langle \text{Log } f \rangle_{0.9982} = 0.83 \pm 0.49$ (yellow line). Bottom panel: factor f as a function of the viewing angle θ_v of the system with respect to the line of sight, and the BLR thickness H/r , assuming a disk-like structure and following Eq. 3 (Decarli et al. 2008). The shaded blue area corresponds to the uncertainty on the value of $\langle \text{Log } f \rangle$ we found in this work.

0.9982: since the BH mass estimate from the fitting procedure increases with the BH spin a (e.g. see Fig. C.11 - C.20), from Eq. 2, it is easy to see that also the factor f increases with a as well. If we assume that the accreting matter around the SMBH spun it up to the maximum allowed value ($a = 0.9982$), then we obtain $\langle \text{Log } f \rangle_{0.9982} = 0.83 \pm 0.49$ at 1σ (yellow line in Fig. 4 top panel).

Following Collin et al. (2006) and Decarli et al. (2008), assuming a disk-like structure for the BLR, the factor f can be expressed as

$$f = \frac{1}{4 \left[\sin^2 \theta_v + \left(\frac{H}{r} \right)^2 \right]}, \quad (3)$$

where θ_v is the inclination angle of the disk with respect the line of sight, and H/r is the ratio between the half-thickness and the radius of the BLR (see Fig. 4, bottom panel). Following this last expression, the disk viewing angle has to be $\theta_v \lesssim 30^\circ$, that is consistent with our approach to consider all the sources observed from an angle $\theta_v < 45^\circ$. Moreover, the ratio H/r is $\lesssim 0.5$, consistent with what Majia-Restrepo et al. (2018) have found.

From Fig. 4, it is easy to notice that the factor f spans a wide range of values (~ 2 orders of magnitude). Despite our finding $\langle \text{Log } f \rangle$ is in agreements with the most common/used values in literature, given the large uncertainties, it is not possible to draw any strong conclusion about its precise value.

4. Conclusions

We used the relativistic thin AD model KERRBB (Li et al. 2005) to infer the observed disk luminosity, the Eddington ratio and the BH mass of 53 sources from the AGN Black Hole Mass Database (Bentz & Katz 2015), from the works of Lira et al. (2018), Grier et al. (2017, 2019) and Hoorman et al. (2019). These sources have: 1] a BH mass estimate from the RM technique; 2] a clear evidence of the UV emission (the so-called 'Big Blue Bump') produced by the radiation coming from an AD around the SMBH, with no contamination from the host galaxy. Since we did not have information about the viewing angle, we assumed to observe these Type 1 QSOs with $\theta_v \leq 45^\circ$ in order to avoid the absorption from the dusty torus (assumed to have an average opening angle of $\sim 45^\circ$); we also showed the correction from the possible extinction of the UV spectrum due to the dust in the host galaxy ISM, following the work of B16. Our results are summarized below:

- The BH mass estimates from the AD fitting procedure are consistent (within the uncertainties) with the ones coming from the RM technique and the same compatibility is present also in the case with SE BH mass estimates (Fig. 2).
 - The mean uncertainty (~ 0.45 dex) related to the AD BH mass estimate is connected to different quantities:
 - BH Spin: the BH mass changes by ~ 0.5 dex going from $a = 0$ to $a = 0.9982$; taking as a reference value the arithmetic mean of the BH mass in this spin range (as done in this work), the uncertainty is ~ 0.25 dex;
 - Viewing angle of the system: for a fixed BH spin, the BH mass changes by ~ 0.2 dex going from $\theta_v = 0^\circ$ to $\theta_v = 45^\circ$; taking as a reference value the arithmetic mean of the BH mass in this viewing angle range, the uncertainty is ~ 0.1 dex;
 - Spectral peak frequency ν_p and luminosity $\nu_p L_{\nu_p}$: on average the uncertainty on both measurements is ~ 0.05 dex, which corresponds to an uncertainty of ~ 0.1 dex on the BH mass;
- If the quality of data is high and either the spectral peak or the viewing angle of the system are well constrained (with an uncertainty of less than $\sim 5\%$), the mean uncertainty on the AD BH mass estimate is ~ 2 , smaller than the systematic uncertainties on both the RM and SE estimates ($\sim 3 - 4$, e.g. Vestergaard & Osmer 2009; Peterson 2010);
- Assuming that the BH mass estimated with the AD fitting procedure is correct, we studied the distribution of the factor f , computed using Eq. 2: we found that the mean (logarithmic) value is $\langle \text{Log } f \rangle = 0.63 \pm 0.49$ at 1σ , consistent within the uncertainties with the most used/common estimate. Despite this compatibility, the involved uncertainties are still large (see Fig. 4) and it is not possible to draw any strong conclusion about its precise value.
 - Assuming that the BLR has a disk-like structure and f can be expressed as in Eq. 3 (following Collin et al. 2006; Decarli et al. 2008), the average geometrical factor found in this work leads to the following results:
 - The viewing angle of the system has to be $\theta_v \lesssim 30^\circ$;
 - The BLR thickness ratio is $H/r < 0.5$, result similar to the one found by Majia-Restrepo et al. (2018).

The good agreement between the RM results (or the ones from the SE relations) with the AD results strengthens the choice of using AD models as an alternative method to infer the mass of SMBHs. Nonetheless the uncertainties on the geometrical factor f , on the SE scaling relations and on the available photometry and spectrometry are still large to have precise information

on the BH accretion and rotation from the comparison between these methods; also the possible influence of disk radiation pressure on the BLR geometry (e.g. Collin et al. 2006; Marconi et al. 2008) and on the disk emission and efficiency can affect the BH mass estimate.

A larger sample of sources with RM measurements and a clear prominent AD emission are needed in order to strengthen these findings and possibly, to have more information on the BH accretion.

References

- Abramowicz M., Czerny B., Lasota J. P., & Szuszkiewicz E., 1988, *ApJ*, 332, 646-658
- Baron, D., Stern, J., Poznanski, D. & Netzer, H., 2016, *APJ*, 832(1),8
- Bentz, M. C., Katz, S., 2015, *PASP*, 127, 67
- Bentz, M. C., Peterson, B. M., Pogge, R. W., Vestergaard, M. & Onken, C. A., 2006, *ApJ*, 644, 133
- Bentz, M. C., et al., 2009, *ApJ*, 705, 199
- Blandford, R. D. & McKee, C. F., 1982, *ApJ*, 255, 419
- Calderone, G., Ghisellini, G., Colpi, M., & Dotti, M., 2013, *MNRAS*, 431, 210
- Calderone, G. et al., 2017, *MNRAS*, 72, 4
- Campitiello, S., Ghisellini, G., Sbarrato, T., & Calderone, G., 2018, *A&A*, 612, A59
- Campitiello, S., Celotti, A., Ghisellini, G. & Sbarrato, T., 2019, *A&A*, 625, A23
- Cardelli, J. A., Clayton, G. C. & Mathis, J. S., 1989, *ApJ*, 345, 245
- Collin, S., Kawagushi, T., Peterson, B. M., & Vestergaard, M., 2006, *A&A*, 456, 75
- Czerny, B., et al., 2004, *MNRAS*, 348(3), L54-L57
- Dai, X. et al., 2010, *ApJ*, 709, 278
- Davies R. I., 2006, *ApJ*, 646, 754
- Davis, S. W. & Laor, A., 2011, *ApJ*, 728, 98
- Decarli, R., Dotti, M., Fontana, M. & Haardt, F., 2008, *MNRAS*, 386, L15-L19
- De Rosa, G. et al., 2007, *ApJ*, 790(2), 145
- Dibai, E. A., 1977, *Soviet Astronomy Letters*, 3, 1
- Dibai, E. A., 1980, *Soviet Astronomy Letters*, 24, 389
- Dibai, E. A., 1984, *Soviet Astronomy Letters*, 28, 245
- Ghisellini, G. et al., 2010, *MNRAS*, 405, 387
- Graham, A. W., Onken, C. A., Athanassoula, E. & Combes, F., 2011, *MNRAS*, 412, 221
- Greene, J. E. & Ho, L. C., 2005, *ApJ*, 630, 122
- Greene, J. E. et al., 2010, *ApJ*, 721, 26
- Grier, C. J. et al., 2013a, *ApJ*, 773, 90
- Grier, C. J. et al., 2013b, *ApJ*, 764, 47
- Grier, C. J. et al., 2017, *ApJ*, 851, 21
- Grier, C., J. et al., 2019, arXiv:1904.03199
- Guerras, E. et al., 2013, *ApJ*, 764(2), 160
- Hicks, E. K. S. & Malkan, M. A., 2008, *ApJS*, 174, 31
- Ho, L. C., 1999, in *Observational Evidence for Black Holes in the Universe*, ed. S. K. Chakrabarti (Dordrecht: Kluwer), 157
- Hoorman, J., K. et al., 2019, arXiv preprint arXiv:1902.04206
- Horne, K., Peterson, B. M., Collier, S. J. & Netzer, H., 2004, *PASP*, 116, 465
- Hubeny, I., Agol, E., Blaes, O., & Krolik, J. H., 2000, *ApJ*, 533, 710
- Irwin, M. J., Webster, R. L., Hewett, P. C., Corrigan, R. T. & Jedrzejewski, R. I., 1989, *AJ*, 98, 1989
- Kaspi, S., Smith, P. S., Netzer, H., Maoz, D., Jannuzi, B. T. & Giveon, U., 2000, *ApJ*, 533, 631
- Kaspi, S., Maoz, D., Netzer, H., Peterson, B. M., Vestergaard, M. & Jannuzi, B. T., 2005, *ApJ*, 629, 61
- Kaspi, S. et al., 2007, *ApJ*, 659, 997
- Kollmeier, J. A. et al., 2006, *ApJ*, 648, 128
- Koratkar, A. & Blaes, O., 1999, *PASP*, 111, 1
- Laor, A., 1990, *MNRAS*, 246, 369
- Laor, A. & Netzer, H., 1989, *MNRAS* 238, 897
- Lewis, G. F., Irwin, M. J., Hewett, P. C. & Foltz, C. B., 1998, *MNRAS*, 295, 573
- Li, L.-X., Zimmerman, E. R., Narayan, R., & McClintock, J. E., 2005, *ApJ*, 157, 335-370
- Lira, P., Kaspi, S., Netzer, H., et al., 2018, *ApJ*, 865, 56
- Mejia-Restrepo, J., E., Trakhtenbrot, B., Lira, P., Netzer, H., & Capellupo, D., M., 2016, *MNRAS*, 460, 187
- Mejia-Restrepo, J. E., et al., 2018 *Nature Astronomy*, 2.1, 63
- Malkan, M. A., 1983, *ApJ*, 268, 582
- Mannucci, F., Basile, F., Poggianti, B. M., Cimatti, A., Daddi E., Pozzetti, L., 2001, *MNRAS*, 326, 745
- Marconi, A., Axon, D., J., Maiolino, R., Nagao, T., Pastorini, G., Pietrini, P., Robinson, A. & Torricelli, G., 2008, *ApJ*, 678, 693

McLure, R. J. & Dunlop, J. S., 2004, MNRAS, 352, 1390
 McLure, R. J. & Jarvis, M. J., 2002, MNRAS, 337, 109
 Morgan, C. W., Kochanek, C. S., Morgan, N. D. & Falco, E. E., 2010, ApJ, 712, 1129
 Mosquera, A. M. & Kochanek, C. S., 2011, ApJ, 738, 96
 Netzer, H., 1990, in Active Galactic Nuclei, ed. T. J.-L. Courvoisier & M. Mayor, 137
 Netzer, H. & Marziani, P., 2010, ApJ, 724, 318–328
 Netzer, H. & Peterson, B. M., 1997, Astrophysics and Space Science Library, 218, 85
 Novikov, I. D. & Thorne, K. S., 1973, in Black holes, ed. C. De Witt and B. De Witt (New York: Gordon and Breach), 343
 Onken, C. A. & Kollmeier, J. A., 2008, ApJ, 689, L13
 Onken, C. A., Ferrarese, L., Merritt, D., Peterson, B. M., Pogge, R. W., Vestergaard, M., & Wandel, A., 2004, ApJ, 615, 645
 Onken, C. A. et al., 2007, ApJ, 670, 105
 Page, D. N. & Thorne, K. S., 1974, ApJ, 191, 507
 Peterson, B. M., 1993, PASP, 105, 247
 Peterson, B. M., 2010, IAU Symposium, 267, 151
 Peterson, B. M. et al., 2004, ApJ, 613, 682
 Popovic, L. C., Mediavilla, E. G. & Muñoz, J. A., 2001, A&A, 378, 295
 Rafiee, A. & Hall, P. B., 2011, ApJS, 194, 42
 Richards, G., T., et al., 2004, ApJ, 610, 679
 Richards, G., T., et al., 2006, ApJS, 166, 470
 Rokaki, E., Boisson, C. & Collin-Souffrin, S., 1992, A&A, 253, 57
 Sadowski A., 2009, ApJS, 183, 171
 Sadowski A., Abramowicz M., Bursa M., Kluzniak W., Rozanska, A., & Straub, O., 2009, A&A, 502, 7
 Sadowski A., Abramowicz M., Bursa M., Kluzniak W., Lasota J.-P. & Rozanska A., 2011, A&A, 527, A17
 Schlegel, D., J., Finkbeiner, D., P. & Davis, M., 1998, ApJ, 500, 525
 Shen, Y. & Liu, X., 2012, ApJ, 753, 125
 Shen, Y. et al., 2011, ApJS, 194, 45
 Sluse, D. et al., 2011, A&A, 528, 100
 Sun, W.-H. & Malkan, M. A., 1989, ApJ, 346, 68
 Trakhtenbrot, B. & Netzer, H., 2012, MNRAS, 427, 3081
 Trevese, D. et al., 2014, ApJ, 795, 164
 Tripp, T. M., Bechtold, J. & Green, R. F., 1994, ApJ, 433, 533
 Tsuzuki, Y., Kawara, K., Yoshii, Y., et al., 2006, ApJ, 650, 57
 Vestergaard, M., 2002, ApJ, 571, 733
 Vestergaard, M. & Osmer, P. S., 2009, ApJ, 699, 800
 Vestergaard, M. & Peterson, B. M., 2006, ApJ, 641, 689
 Vestergaard, M., & Wilkes, B. J., 2001, ApJS, 134, 1
 Wandel, A. & Petrosian, V., 1988, ApJ, 329, L11
 Wandel, A., Peterson, B. M. & Malkan, M. A., 1999, ApJ, 526, 579
 Wang, J. G. et al., 2009, ApJ, 707, 1334
 Woo, J.-H., Yoon, Y., Park, S., Park, D. & Kim, S., C., 2015, ApJ, 801, 38
 Wu, X.-B., Wang, R., Kong, M. Z., Liu, F. K. & Han, J. L., 2004, A&A, 424, 793

Appendix A: Sample data

Our sample is made of sources already present in other works: the AGN Black Hole Mass Database (Bentz & Katz 2015), the work of Lira et al. (2018), Grier et al. (2017, 2019). We chose 53 sources (21 from the AGN Database, 9 from Lira et al. 2018, 4 from Grier et al. 2017 and 19 from Grier et al. 2019) with a visible UV bump produced by the AD around the SMBH, whose SED is not contaminated by the host galaxy emission; we also selected the ones whose RM BH mass estimate has an uncertainty of less than 50%.

Tables A.1 - A.2 show the whole sample and the data we used in this work. The sample is divided in 6 sub-samples, based on the spectral quality and availability: [A] sources whose available spectrum covers the whole rest-frame range $\lambda = 1000 - 10000 \text{ \AA}$; [B] sources whose available spectrum covers the whole rest-frame range $\lambda = 1000 - 10000 \text{ \AA}$ except the MgII line region ($\lambda \sim 2000 - 4000 \text{ \AA}$); [C] sources whose available spectrum covers the rest-frame range $\lambda = 2500 - 10000 \text{ \AA}$ (H β and MgII line regions): we used the curvature of the available spectrum to infer the peak position; [D] sources for which we adopted the largest extinction $E_{B-V} (\geq 0.07)$ in order to correct the spectrum from ISM dust absorption; [E] sources whose available spectrum covers only the CIV and MgII line regions ($\lambda < 3000 \text{ \AA}$). In the two tables, we reported:

1. Name of the sources (see the Table caption for details about the references);
2. Redshift;
3. BH mass in solar masses from RM with a geometrical factor $f = 4$ (see the Table caption for details about the references). The reported uncertainty is related to the uncertainty on the light-travel time and the line velocity dispersion (see the reference works for further details);
4. Line velocity dispersion in km/s;
5. Light-travel time in the rest-frame expressed in days;
6. SE BH mass in solar masses (see the Table caption for more details); the systematic uncertainty is ~ 0.5 dex, comparable to the systematic one related to the RM estimates (Vestergaard & Osmer 2009);
7. Observed disk luminosity estimated from the fit;
8. BH mass in solar masses estimates from the fitting procedure;
9. Eddington ratio from the fit (for 5 sources we performed another fit after the correction from dust, from which we reported the new estimates for L_d^{obs} , M and λ);
10. Correction from dust computed using the expression in Baron et al. (2016) (see text): for group [E], E_{B-V} is not present because no spectroscopic data are available in the range $3000\text{-}5000 \text{ \AA}$ in order to compute the observed spectrum slope α_ν (see Sect. 2).

Appendix B: KERRBB equations

The relativistic model KERRBB (Li et al. 2005) describes the emission produced by a thin disk around a Kerr BH. The authors included all relativistic effects such as frame-dragging, Doppler beaming and light-bending. Campitiello et al. (2018) build an analytic approximation of the KERRBB disk emission features considering an hardening factor equal to 1 and no limb-darkening effect: in the case of a face-on disk, they found analytic expressions to compute the BH mass M and accretion rate \dot{M} by fitting a given SED for different spin values. From the SED, the spectrum peak ν_p , peak luminosity $\nu_p L_{\nu_p}$ and observed disk luminosity L_d^{obs} are

$$\frac{\nu_p}{[\text{Hz}]} = \mathcal{A} \left[\frac{\dot{M}}{M_{\odot, \text{yr}^{-1}}} \right]^{1/4} \left[\frac{M}{10^9 M_{\odot}} \right]^{-1/2} g_1(a, \theta_v), \quad (\text{B.1})$$

$$\frac{\nu_p L_{\nu_p}}{[\text{erg/s}]} = \mathcal{B} \left[\frac{\dot{M}}{M_{\odot, \text{yr}^{-1}}} \right] \cos \theta_v g_2(a, \theta_v), \quad (\text{B.2})$$

$$L_d^{\text{obs}} = \mathcal{F}(\theta_v, a) \eta(a) \dot{M} c^2 \sim 2\nu_p L_{\nu_p}, \quad (\text{B.3})$$

where $\text{Log } \mathcal{A} = 15.25$, $\text{Log } \mathcal{B} = 45.66$, η is the disk radiative efficiency and \mathcal{F} is a function depending on the viewing angle θ_v and the BH spin a , that contains all the general relativistic modifications. Notice that the total disk luminosity $L_d = \eta \dot{M} c^2$ is different than the observed disk luminosity (i.e. the frequency integrated AD luminosity) $L_d^{\text{obs}} = \int L_\nu d\nu$ because of relativistic effect described by \mathcal{F} (see Campitiello et al. 2018 for details). \mathcal{F} , g_1 and g_2 have an analytical form reported in Campitiello et al. (2018, 2019) for the viewing angles $\theta_v = 0^\circ - 30^\circ - 45^\circ$. Then, by inverting Eqs. B.1 - B.2, it is possible to find the BH mass and Eddington ratio (defined as $\lambda_{\text{Edd}} = \eta \dot{M} c^2 / C(M/M_{\odot})$, where $C = 1.26 \cdot 10^{38} \text{ erg/s}$):

$$\frac{M}{M_{\odot}} = \mathcal{D} \frac{[g_1(a, \theta_v)]^2}{\sqrt{\cos \theta_v g_2(a, \theta_v)}} \frac{\sqrt{\nu_p L_{\nu_p}}}{\nu_p^2}, \quad (\text{B.4})$$

Group	Source Name	Redshift	Log $M_{\text{BH, RM}}$ ($f = 4$)	σ (km/s)	τ (days)	Log $M_{\text{BH, SE}}$	Log $L_{\text{d, FIT}}^{\text{obs}}$ (erg/s)	Log $M_{\text{BH, FIT}}$	$\lambda_{\text{Edd, FIT}}$	E_{B-V}
	(1)	(2)	(3)	(4)	(5)	(6)	(7)	(8)	(9)	(10)
	3C273	0.158	8.87 ^{+0.11} _{-0.18}	1777 ± 150	306.8 ^{+68.5} _{-90.9}	8.69	46.68 ^{+0.07} _{-0.05}	9.18 ± 0.46	0.23 ± 0.11	0.03
	Fairall 9	0.047	8.28 ^{+0.08} _{-0.14}	3787 ± 197	17.4 ^{+3.2} _{-4.3}	8.55	44.92 ^{+0.05} _{-0.05}	8.31 ± 0.43	0.03 ± 0.01	0.01
	MRK 1383	0.086	8.94 ^{+0.13} _{-0.24}	3442 ± 308	95.0 ^{+29.9} _{-37.1}	8.79	45.49 ^{+0.06} _{-0.05}	8.47 ± 0.44	0.07 ± 0.04	0.03
[A]	MRK 1501	0.089	8.03 ^{+0.12} _{-0.16}	3321 ± 107	12.6 ^{+3.9} _{-3.9}	8.48	45.04 ^{+0.09} _{-0.05}	8.39 ± 0.45	0.03 ± 0.02	0.03
	PG 0052+251	0.154	8.34 ^{+0.11} _{-0.15}	1783 ± 86	89.8 ^{+24.5} _{-24.1}	8.52	45.70 ^{+0.10} _{-0.05}	8.75 ± 0.44	0.06 ± 0.03	0.05
	PG 0844+349	0.064	7.82 ^{+0.15} _{-0.23}	1448 ± 79	12.2 ^{+5.2} _{-1.3}	8.04 ^a	45.03 ^{+0.08} _{-0.05}	8.49 ± 0.45	0.03 ± 0.01	0.04
	PG 0953+414	0.234	8.30 ^{+0.10} _{-0.13}	1306 ± 144	150.1 ^{+21.6} _{-22.6}	8.43	46.16 ^{+0.12} _{-0.05}	8.89 ± 0.44	0.13 ± 0.07	0.05
	MRK 876	0.129	88.30 ^{+0.16} _{-0.27}	2547 ± 342	40.1 ^{+15.0} _{-15.2}	8.32 ^b	45.67 ^{+0.08} _{-0.05}	8.85 ± 0.45	0.05 ± 0.03	0.04
[B]	PG 0804+761	0.100	8.64 ^{+0.07} _{-0.08}	1971 ± 105	146.9 ^{+18.8} _{-18.9}	8.52 ^b	45.67 ^{+0.07} _{-0.05}	8.63 ± 0.43	0.08 ± 0.04	0.02
	PG 1307+085	0.155	8.43 ^{+0.14} _{-0.27}	1820 ± 122	105.6 ^{+36.0} _{-46.6}	8.71	45.53 ^{+0.06} _{-0.05}	8.71 ± 0.43	0.05 ± 0.02	0.03
	(_{G17}) SDSSJ141856.19+535845.0	0.976	8.84 ^{+0.18} _{-0.21}	3220 ± 70	15.8 ^{+6.0} _{-1.9}	8.70	46.14 ^{+0.05} _{-0.05}	9.04 ± 0.43	0.09 ± 0.05	0.01
[C]	(_{G17}) SDSSJ141941.11+533649.6	0.646	7.55 ^{+0.16} _{-0.25}	1232 ± 30	30.4 ^{+3.9} _{-8.3}	8.20	45.43 ^{+0.05} _{-0.05}	8.64 ± 0.43	0.04 ± 0.02	0.01
	(_{G17}) SDSSJ142052.44+525622.4	0.676	8.67 ^{+0.14} _{-0.20}	7195 ± 40	11.9 ^{+1.3} _{-1.0}	8.50	45.87 ^{+0.05} _{-0.05}	8.84 ± 0.43	0.08 ± 0.04	0.01
	MRK 142	0.449	7.19 ^{+0.07} _{-0.10}	972 ± 12	7.9 ^{+1.2} _{-1.1}	6.95	44.22 ^{+0.05} _{-0.05}	8.21 ± 0.43	~ 0.01	0.07
	MRK 335	0.026	7.19 ^{+0.04} _{-0.04}	948 ± 113	12.5 ^{+6.6} _{-5.5}	7.37 ^a	44.38 ^{+0.05} _{-0.05}	8.11 ± 0.43	~ 0.01	0.22
	MRK 877	0.112	8.58 ^{+0.16} _{-0.30}	2626 ± 211	71.5 ^{+29.6} _{-33.7}	8.23	44.93 ^{+0.05} _{-0.05}	8.17 ± 0.43	~ 0.01	0.22
[D]	PG 0026+129	0.142	8.43 ^{+0.14} _{-0.23}	1773 ± 285	111.0 ^{+24.1} _{-28.3}	7.83	45.14 ^{+0.12} _{-0.05}	8.94 ± 0.49	~ 0.01	0.07
	PG 1211+143	0.081	8.42 ^{+0.16} _{-0.28} *	1832 ± 81	103 ⁺³² ₋₄₄	7.67 ^a	45.70 ^{+0.10} _{-0.05}	8.62 ± 0.44	0.09 ± 0.04	0.07
	PG 1411+442	0.089	8.39 ^{+0.19} _{-0.34}	1607 ± 169	124.3 ^{+61.0} _{-61.7}	7.92	45.25 ^{+0.14} _{-0.06}	8.90 ± 0.48	0.02 ± 0.01	0.07
	PG 1700+518	0.292	8.75 ^{+0.09} _{-0.10}	1700 ± 123	251.8 ^{+45.9} _{-38.8}	8.21	45.16 ^{+0.05} _{-0.05}	8.80 ± 0.43	~ 0.01	0.09
	PG 2130+099	0.063	7.91 ^{+0.06} _{-0.07}	1825 ± 65	31.0 ^{+4.0} _{-4.0}	7.62	45.37 ^{+0.05} _{-0.05}	8.69 ± 0.43	0.03 ± 0.02	0.11
	(_{G17}) SDSSJ141859.75+521809.7	0.884	7.99 ^{+0.16} _{-0.28}	2491 ± 26	20.4 ^{+5.6} _{-7.0}	8.80	46.08 ^{+0.17} _{-0.05}	9.44 ± 0.56	0.03 ± 0.02	0.11
	Ark 120	0.327	8.81 ^{+0.05} _{-0.10}	1884 ± 48	29.7 ^{+3.3} _{-3.9}	8.14	45.09 ^{+0.15} _{-0.05}	8.53 ± 0.43	0.03 ± 0.01	0.07
	PG 1247+267	2.038	9.64 ^{+0.15} **	4939 ± 117	142 ⁺²⁶ ₋₂₅	9.88 ^b	45.41 ^{+0.05} _{-0.05}	9.05 ± 0.43	~ 0.01	0.07
	S5 0836+71	2.172	10.14 ^{+0.06} ***	9700	188 ⁺²⁷ ₋₃₇	9.59 ^b	45.54 ^{+0.05} _{-0.05}	8.78 ± 0.44	~ 0.01	-
	(_L) CT286	2.556	10.14 ^{+0.08} _{-0.07}	6256	459 ⁺⁹² ₋₇₁	9.35	47.87 ^{+0.05} _{-0.05}	9.88 ± 0.43	0.70 ± 0.35	-
	(_L) CT320	2.956	8.71 ^{+0.40} _{-0.16}	3493	55 ⁺⁸⁴ ₋₁₇	9.79	47.54 ^{+0.05} _{-0.05}	9.52 ± 0.43	0.73 ± 0.33	-
	(_L) CT406	3.183	9.53 ^{+0.25} _{-0.34}	6236	115 ⁺⁸⁶ ₋₆₄	9.68	47.39 ^{+0.05} _{-0.05}	9.52 ± 0.43	0.53 ± 0.28	-
	(_L) CT650	2.662	9.16 ^{+0.03} _{-0.09}	3419	162 ⁺¹⁰ ₋₃₃	9.27	47.13 ^{+0.05} _{-0.05}	9.33 ± 0.43	0.46 ± 0.22	-
	(_L) CT953	2.535	9.47 ^{+0.15} _{-0.09}	5506	127 ⁺⁵³ ₋₂₄	9.77	47.23 ^{+0.05} _{-0.05}	9.52 ± 0.43	0.38 ± 0.18	-
[E]	(_L) CT975	2.866	9.32 ^{+0.05} _{-0.34}	5970	77 ⁺⁹ ₋₄₂	9.73	47.23 ^{+0.05} _{-0.05}	9.58 ± 0.43	0.32 ± 0.16	-
	(_L) HB890329-385	2.433	10.12 ^{+0.05} _{-0.13}	6275	438 ⁺⁴⁸ ₋₁₁₃	9.83	47.29 ^{+0.05} _{-0.05}	9.63 ± 0.43	0.30 ± 0.15	-
	(_L) 2QZJ214355	2.620	9.67 ^{+0.21} _{-0.54}	6895	128 ⁺⁸² ₋₉₁	9.75	47.08 ^{+0.05} _{-0.05}	9.43 ± 0.43	0.32 ± 0.16	-
	(_L) 2QZJ221516	2.706	9.64 ^{+0.04} _{-0.39}	5888	165 ⁺¹³ ₋₉₈	9.19	47.26 ^{+0.05} _{-0.05}	9.46 ± 0.43	0.46 ± 0.22	-
	(_{G19}) SDSSJ141437.04+530422.7	1.464	8.67 ^{+0.17} _{-0.26}	2144 ± 46	131.1 ^{+42.9} _{-36.6}	-	47.50 ^{+0.05} _{-0.05}	9.59 ± 0.43	0.59 ± 0.29	-
	(_{G19}) SDSSJ141420.55+532216.6	2.216	9.35 ^{+0.13} _{-0.22} ***	3900 ± 34	188.4 ^{+15.6} _{-29.0}	9.11	45.38 ^{+0.05} _{-0.05}	8.68 ± 0.43	0.04 ± 0.02	-
	(_{G19}) SDSSJ141721.81+530454.3	1.930	8.66 ^{+0.14} _{-0.19}	1682 ± 12	208.3 ^{+10.6} _{-10.6}	8.33	46.21 ^{+0.05} _{-0.05}	8.99 ± 0.43	0.12 ± 0.06	-
	(_{G19}) SDSSJ141229.66+531431.7	2.300	9.22 ^{+0.14} _{-0.19}	3412 ± 30	186.1 ^{+5.9} _{-7.4}	8.63	45.75 ^{+0.05} _{-0.05}	8.68 ± 0.43	0.08 ± 0.04	-
	(_{G19}) SDSSJ141735.33+523851.4	1.960	9.51 ^{+0.14} _{-0.22}	4324 ± 36	224.3 ^{+12.4} _{-37.9}	8.39	45.67 ^{+0.05} _{-0.05}	8.60 ± 0.43	0.08 ± 0.04	-
							45.97 ^{+0.05} _{-0.05}	8.63 ± 0.43	0.16 ± 0.08	-

Table A.1. (1) Name of the sources (_(L) from Lira et al. 2018; _(G17) from Grier et al. 2017; _(G19) from Grier et al. 2019; _(H19) from Hoorman et al. 2019; the others from the database of Bentz & Katz 2015); (2) Redshift; (3) BH mass in solar masses from RM with $f = 4$ (average value between the two extreme, most used/common values in literature, $f = 2.8 \pm 0.6$ and $f = 5.5 \pm 1.8$ - Onken et al. 2004; Graham et al. 2011, respectively), using the results reported in the corresponding reference paper (see text for what concerns the uncertainties); (4) line dispersion velocity in km/s; (5) light-travel time in the rest-frame expressed in days; (6) SE BH mass in solar masses computed using the H β line (^a MgII line; ^b CIV line; SE BH masses from Lira et al. (2018), Grier et al. (2019) and Hoorman et al. (2019) are computed using the CIV line; SE BH masses from Grier et al. (2017) are computed using the H β line and the calibration of Vestergaard & Peterson (2006)); (7) (8) (9) observed disk luminosity, BH mass in solar masses and Eddington ratio estimated from the fit (the mass is estimated assuming the BH spin range $0 < a < 0.9982$, the viewing angle range $0^\circ < \theta_v < 45^\circ$ and the uncertainty on the spectrum peak position; the Eddington ratio is estimated by considering only the spin and viewing angle ranges: by including the uncertainty on the spectrum peak position, its overall uncertainty grows by a factor ~ 1.3); for 4 sources we performed another fit after the correction from dust and reported the new estimates for these quantities; (10) correction from dust computed using the expression in Baron et al. (2016) (see text).

Group	Source Name	Redshift	Log $M_{\text{BH, RM}}$ ($f = 2.8$)	σ (km/s)	τ (days)	Log $M_{\text{BH, SE}}$	Log $L_{\text{d, FIT}}^{\text{obs}}$ (erg/s)	Log $M_{\text{BH, FIT}}$	$\lambda_{\text{Edd, FIT}}$	E_{B-V}
(1)	(2)	(3)	(4)	(5)	(6)	(7)	(8)	(9)	(10)	
(G19)	SDSSJ141843.30+531920.8	2.300	$9.03^{+0.15}_{-0.24}$	2792 ± 19	$179.4^{+31.2}_{-42.3}$	8.90	$45.96^{+0.05}_{-0.05}$	8.63 ± 0.43	0.16 ± 0.08	-
(G19)	SDSSJ141818.45+524356.0	2.137	$9.21^{+0.14}_{-0.19}$	3408 ± 16	$180.9^{+4.7}_{-4.7}$	8.76	$45.77^{+0.05}_{-0.05}$	8.39 ± 0.43	0.17 ± 0.09	-
(G19)	SDSSJ142005.59+530036.7	1.645	$8.95^{+0.14}_{-0.20}$	3803 ± 18	$80.4^{+6.3}_{-7.5}$	-	$46.23^{+0.05}_{-0.05}$	8.60 ± 0.43	0.30 ± 0.15	-
(G19)	SDSSJ141347.87+521204.9	2.352	$8.88^{+0.14}_{-0.20}$	2446 ± 19	$163.8^{+8.2}_{-5.3}$	8.87	$46.05^{+0.05}_{-0.05}$	8.53 ± 0.43	0.24 ± 0.11	-
(G19)	SDSSJ141843.67+535138.5	1.589	$8.71^{+0.18}_{-0.21}$	3055 ± 29	$71.9^{+23.8}_{-11.3}$	-	$45.32^{+0.05}_{-0.05}$	8.45 ± 0.43	0.05 ± 0.03	-
(G19)	SDSSJ141730.52+521019.4	1.860	$9.10^{+0.14}_{-0.21}$	4605 ± 37	$76.4^{+6.8}_{-8.7}$	8.91	$45.82^{+0.05}_{-0.05}$	8.42 ± 0.43	0.18 ± 0.09	-
(G19)	SDSSJ141839.03+521333.0	1.850	$9.46^{+0.13}_{-0.20}$	4064 ± 15	$224.3^{+7.1}_{-18.0}$	8.97	$45.95^{+0.05}_{-0.05}$	8.76 ± 0.43	0.11 ± 0.05	-
(G19)	SDSSJ140957.28+535047.0	1.822	$8.61^{+0.17}_{-0.23}$	3321 ± 12	$47.4^{+15.2}_{-8.9}$	8.55	$45.85^{+0.05}_{-0.05}$	8.73 ± 0.43	0.09 ± 0.05	-
[E]	SDSSJ141912.47+520818.0	2.562	$9.21^{+0.15}_{-0.20}$	3961 ± 41	$133.4^{+22.6}_{-5.2}$	9.33	$46.44^{+0.05}_{-0.05}$	9.03 ± 0.43	0.19 ± 0.09	-
(G19)	SDSSJ141101.51+520402.1	2.080	$8.95^{+0.14}_{-0.20}$	2409 ± 45	$197.9^{+9.7}_{-6.6}$	8.39	$45.97^{+0.05}_{-0.05}$	8.49 ± 0.43	0.22 ± 0.10	-
(G19)	SDSSJ141004.22+540109.0	2.325	$9.09^{+0.15}_{-0.23}$	3085 ± 26	$168.5^{+20.4}_{-35.9}$	8.37	$45.77^{+0.05}_{-0.05}$	8.43 ± 0.38	0.15 ± 0.07	-
(G19)	SDSSJ141948.09+520610.5	1.706	$8.87^{+0.14}_{-0.20}$	2229 ± 35	$194.0^{+20.4}_{-12.2}$	8.71	$45.93^{+0.05}_{-0.05}$	8.67 ± 0.43	0.13 ± 0.06	-
(G19)	SDSSJ140913.79+515841.6	2.134	$8.38^{+0.16}_{-0.20}$	2203 ± 27	$64.7^{+12.6}_{-6.3}$	8.67	$45.82^{+0.05}_{-0.05}$	8.58 ± 0.43	0.12 ± 0.06	-
(G19)	SDSSJ141425.95+513801.6	2.332	$8.89^{+0.15}_{-0.21}$	3405 ± 40	$87.2^{+13.9}_{-11.0}$	9.06	$45.89^{+0.05}_{-0.05}$	8.81 ± 0.43	0.09 ± 0.04	-
(H19)	DES J003352.72-425452.60	2.593	$9.45^{+0.06}_{-0.15}$	6250 ± 64	95^{+16}_{-23}	9.52	$46.85^{+0.05}_{-0.05}$	9.18 ± 0.44	0.34 ± 0.16	-
(H19)	DES J022828.19-040044.30	1.905	$9.60^{+0.11}_{-0.16}$	6365 ± 66	123^{+43}_{-42}	9.64	$46.79^{+0.05}_{-0.05}$	9.21 ± 0.44	0.30 ± 0.15	-

Table A.2. As Table A.1.

$$\lambda_{\text{Edd}} = \mathcal{E} \frac{\eta(a)}{g_1^2(a, \theta_v) \sqrt{\cos \theta_v} g_2(a, \theta_v)} \nu_p^2 \sqrt{\nu_p L_{\nu_p}}, \quad (\text{B.5})$$

where $\text{Log } \mathcal{D} = 16.67$ and $\text{Log } \mathcal{E} = -53.675$. As noted before, for high luminous QSOs the thin disk approximation breaks down due to the non-negligible disk vertical structure, and KERRBB results are no longer trustworthy. Another relativistic thin AD model is SLIMBH (Abramowicz et al. 1988; Sadowski 2009; Sadowski et al. 2009; Sadowski et al. 2011) which accounts for the vertical structure of the disk and more appropriate for bright disks (see Koratkar & Blaes 1999); however Campitiello et al. (2019) showed that, given the similarity of the two models, for a fixed spectrum peak, the differences in the estimated masses and Eddington ratios are by a factor of $\lesssim 1.2$.

Appendix C: Fit, BH mass and Eddington ratio

In this section, we show the fit of the individual optical-UV SED (Figs. C.1 - C.10), performed by adapting the KERRBB model (blue thick line) to the rest-frame spectrum (black line) of each source in order to infer the spectrum peak frequency ν_p and luminosity $\nu_p L_{\nu_p}$. Photometric data (red dots) are not used in the fitting procedure because they might be contaminated by emission lines or some kind of absorption. Along with the KERRBB best fit, we show a confidence interval (blue shaded area) that defines a confidence interval for the BH mass: for the majority of our sample, this shaded area includes also the new fit performed by adapting the KERRBB model to the spectrum corrected by the ISM dust (gray line); for some sources we used a large extinction E_{B-V} ($\gtrsim 0.7$, also shown for each source) and we show the new fit (blue dotted line) with the new confidence interval. Each plot is marked with a coloured square: green, if the spectrum is rather good (with a small correction from dust absorption) and the spectral peak position is well constrained; yellow, if we adopted a large correction for the dust absorption or the quality of the spectrum is low.

For each individual source, Figs. C.11 - C.20 show the BH mass as a function of the spin in the range $0 \leq a \leq 0.9982$, for the viewing angles $\theta_v = 0^\circ$ (red dashed line), $\theta_v = 30^\circ$ (blue dashed line), $\theta_v = 45^\circ$ (green dashed line). On each plot, a blue shaded area defines the confidence interval on each estimate. On the same plot, we represented the BH mass estimates coming from RM with a yellow shaded area, assuming $f = 2.8$ and $f = 5.5$ (the thickness of these areas is related to the uncertainty coming from the light-travel time and the line velocity dispersion); when they are not present, an arrow indicates that the RM estimate is smaller/larger than our estimate. On each plot, the Eddington ratio is shown as a function of the BH spin, using the same color code. For the sources for which we used a large extinction E_{B-V} , we plotted also the results coming from the new fit of the spectrum corrected from ISM dust, marked by a shaded red area.

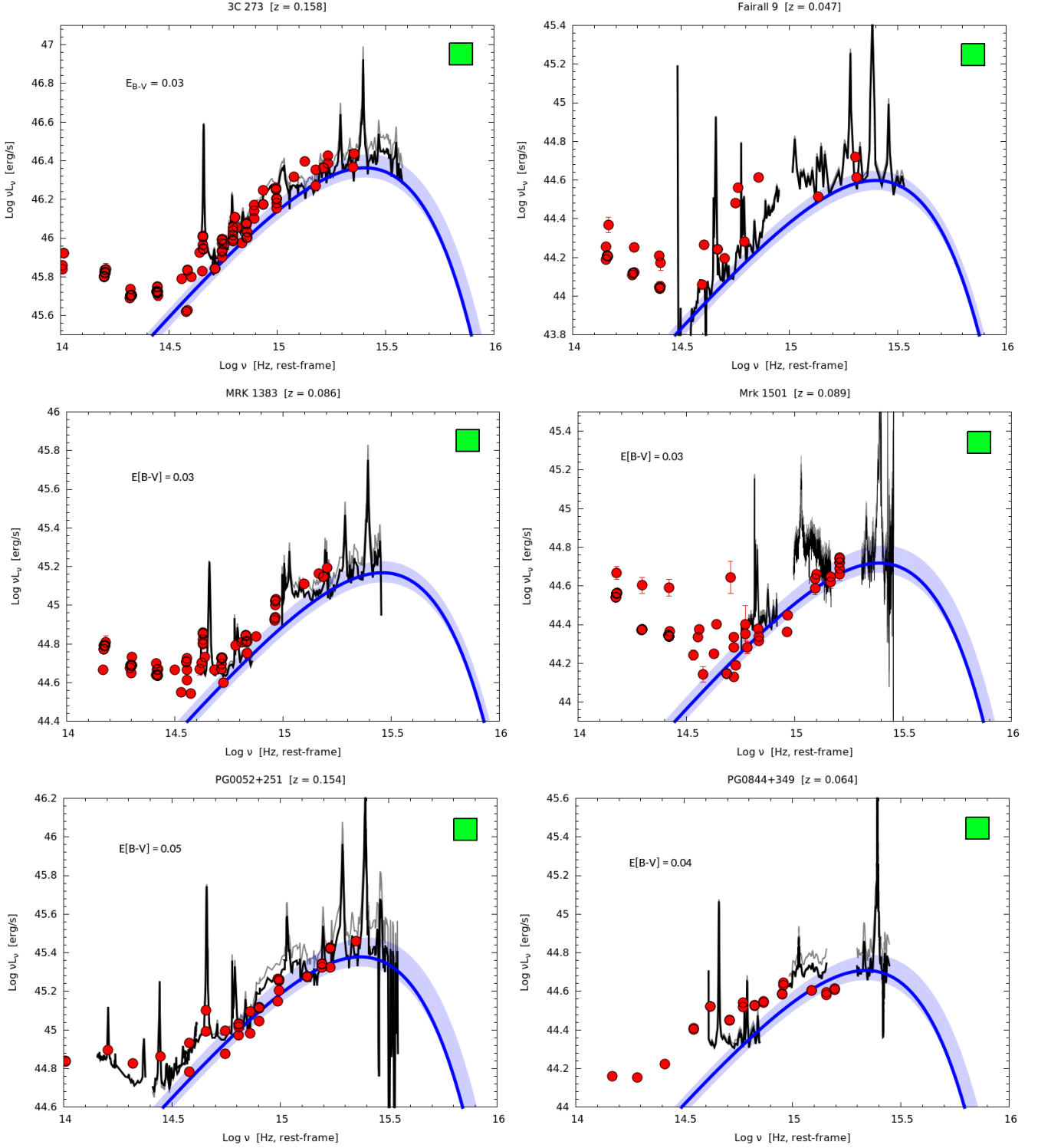


Fig. C.1. Fit of the rest-frame spectrum with the KERRBB model (thick blue line). The blue shaded area is the confidence interval of the best fit model that also includes the fit of the spectrum corrected from dust absorption (gray line) following the procedure described in Sect. 2 (the adopted extinction is reported on each plot). For MRK142, MRK335, PG1411+442 and SDSSJ141859.75+521809.7 we used a large extinction E_{B-V} and we show the new KERRBB fit (blue dotted line) with the new confidence interval. Each plot is marked with a coloured square: green, if the spectrum is rather good (with a small correction from dust absorption) and the spectral peak position is well constrained; yellow, if we adopted a large correction for the dust absorption or the quality of the spectrum is low. Photometry (red dots, with no correction from ISM dust) and spectrometry (black line) come from the literature and public archives. In order to have a 'normalized' and clear SED representation, each plot is constructed in this way: the x-axis is in the range $\text{Log } \nu$ [Hz] = 14 – 16; the y-axis is constructed by taking as the lower y-value the luminosity of the AD model at $\text{Log } \nu$ [Hz] \sim 14.5, and as the upper y-value the lower y-value plus 1.6 dex.

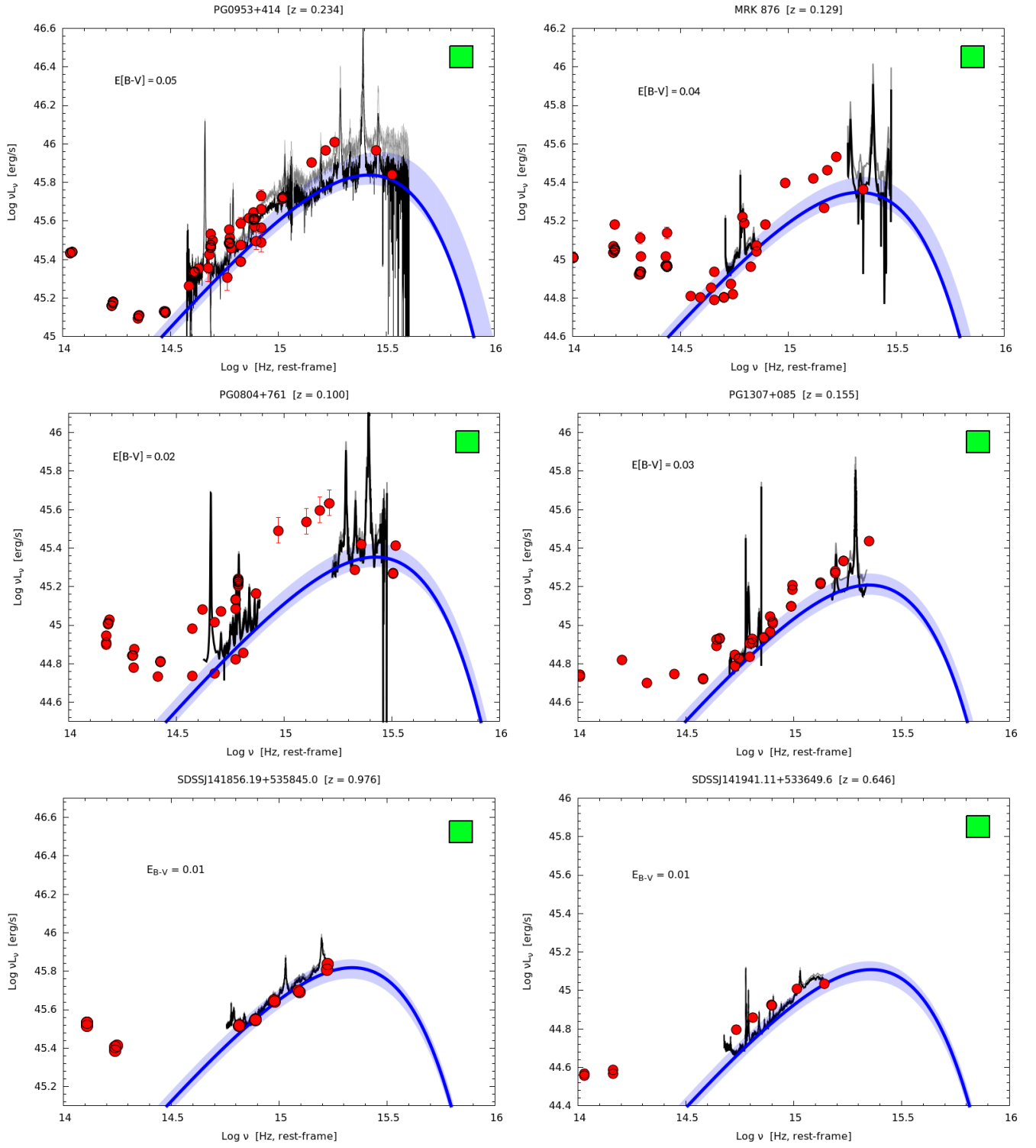


Fig. C.2. (continued).

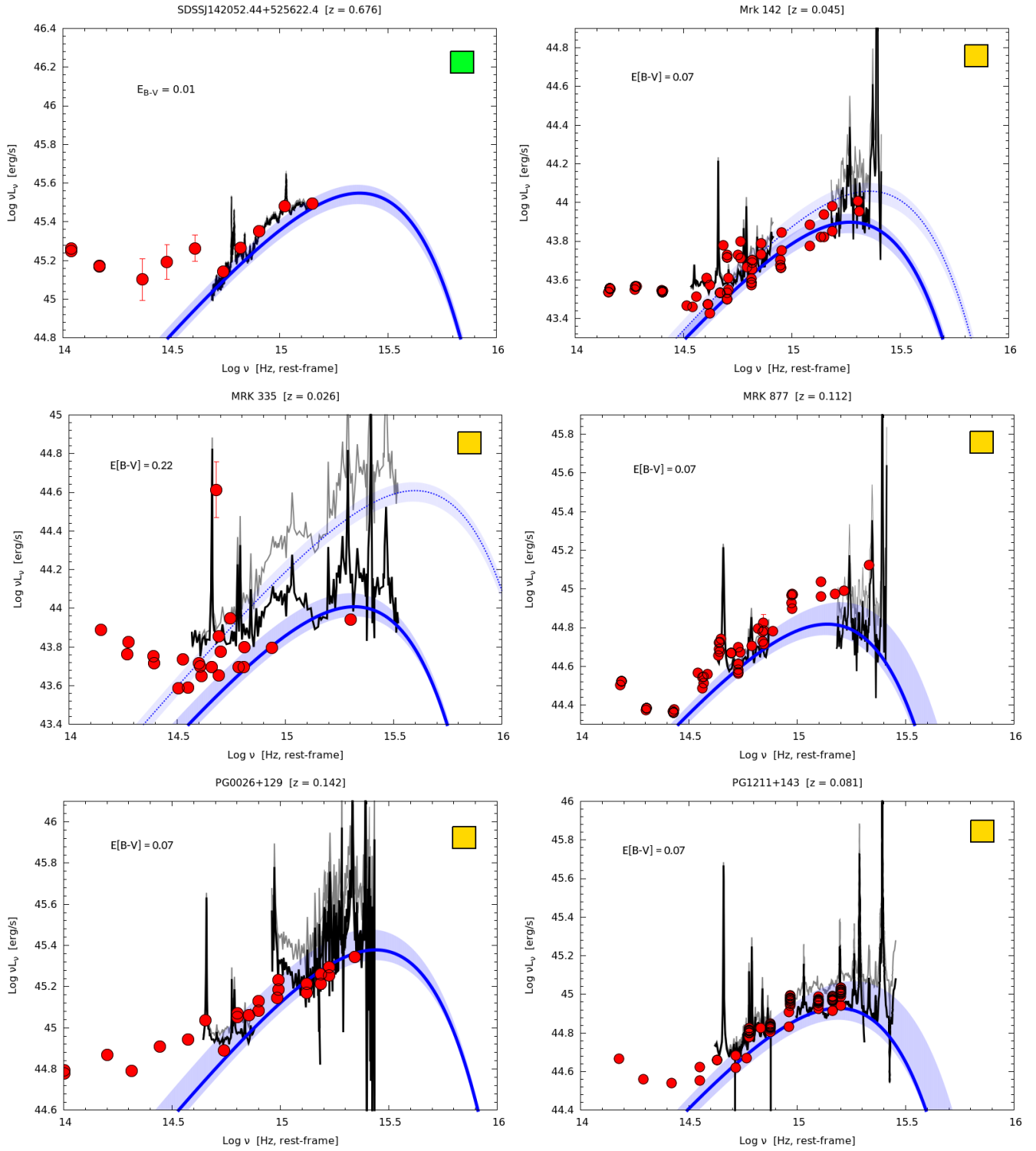


Fig. C.3. continued.

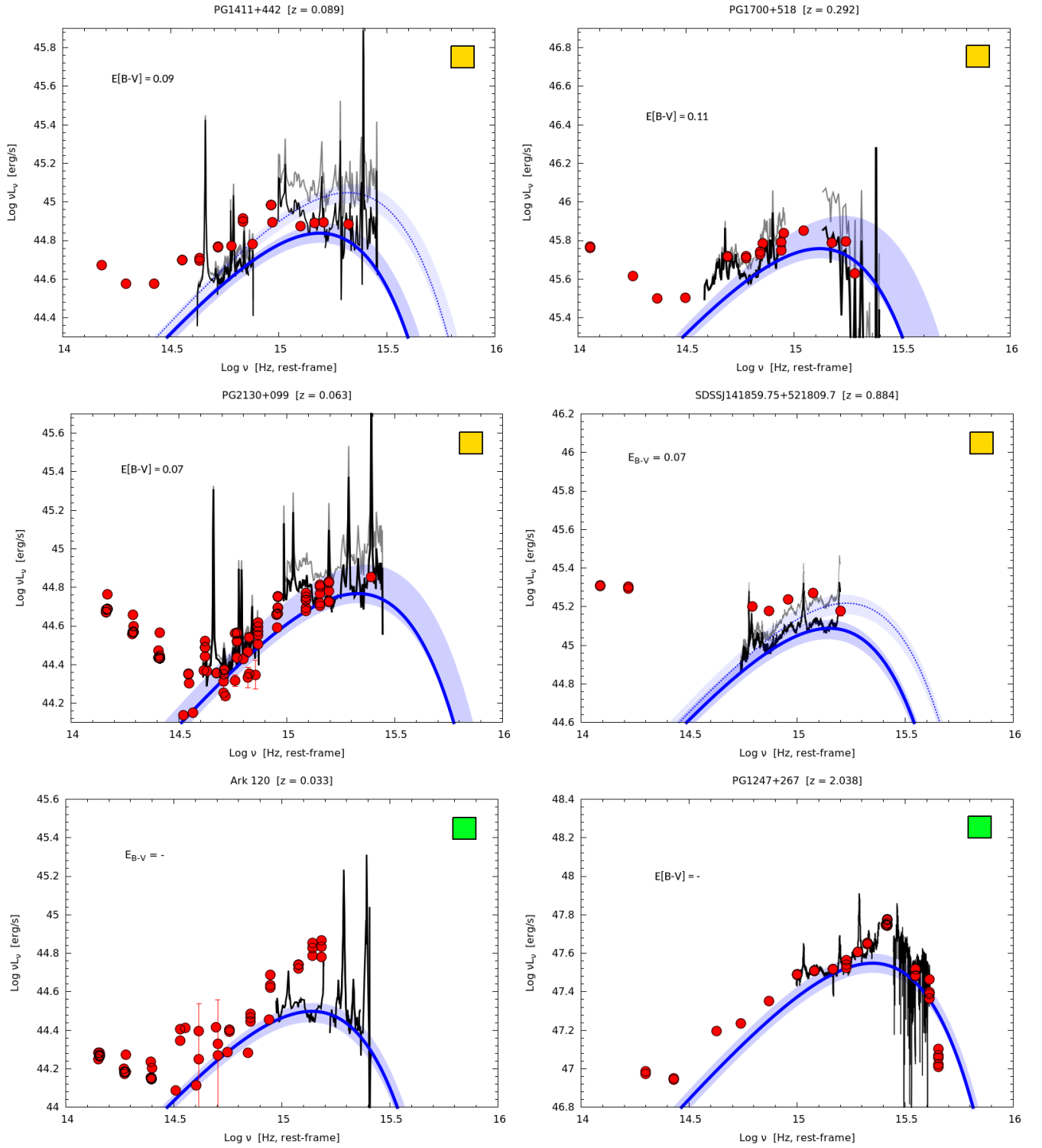


Fig. C.4. continued.

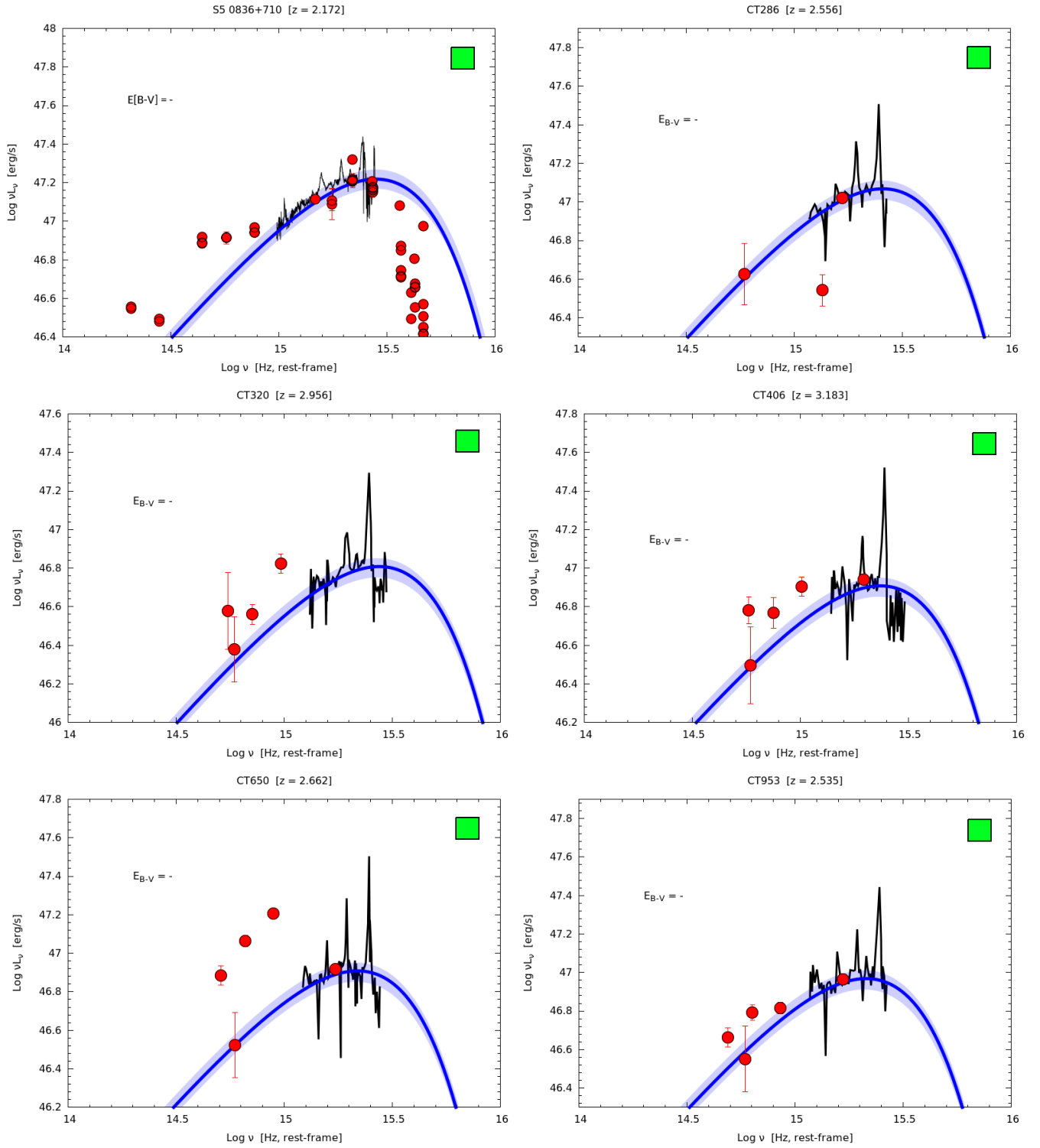


Fig. C.5. continued.

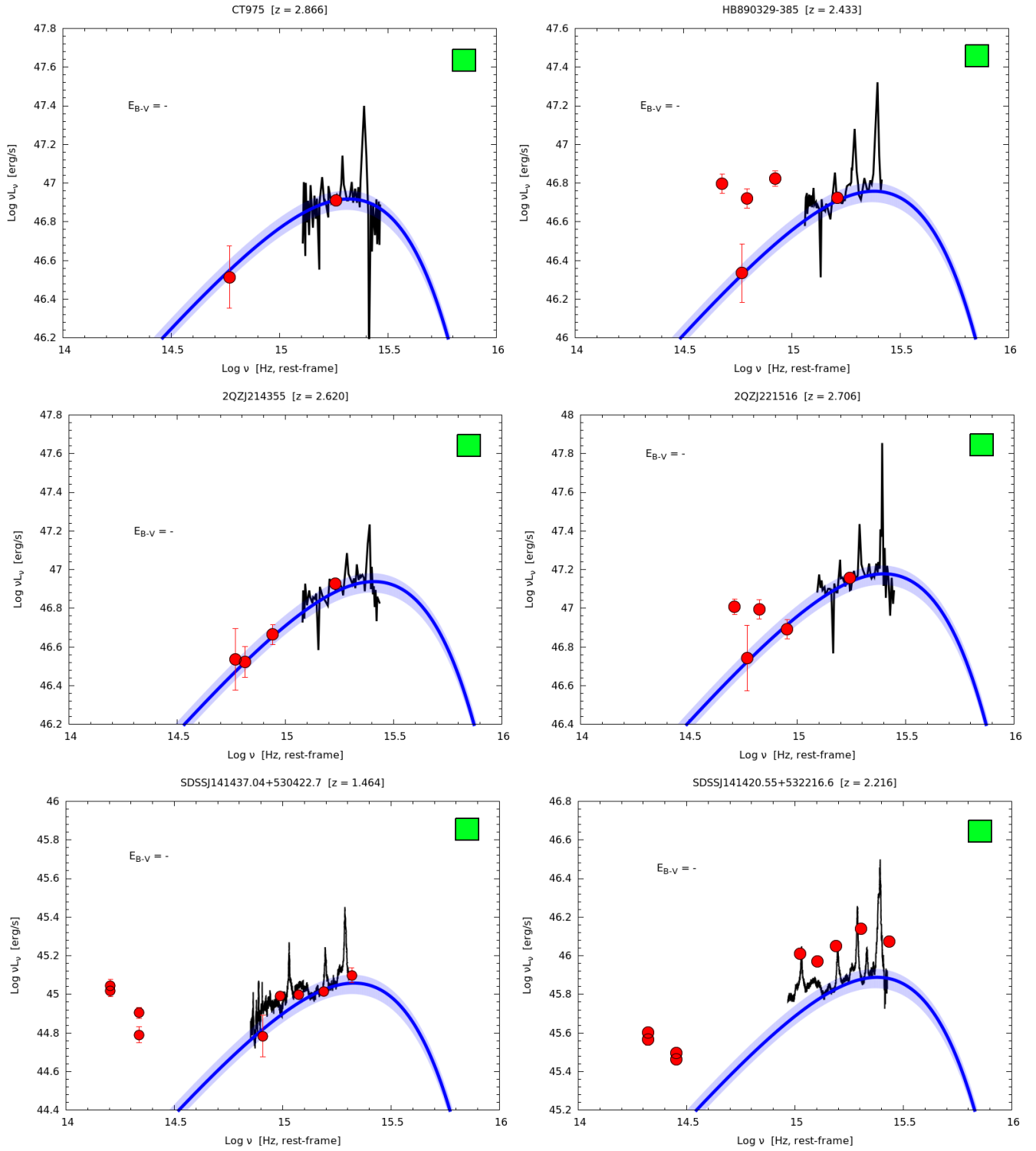


Fig. C.6. continued.

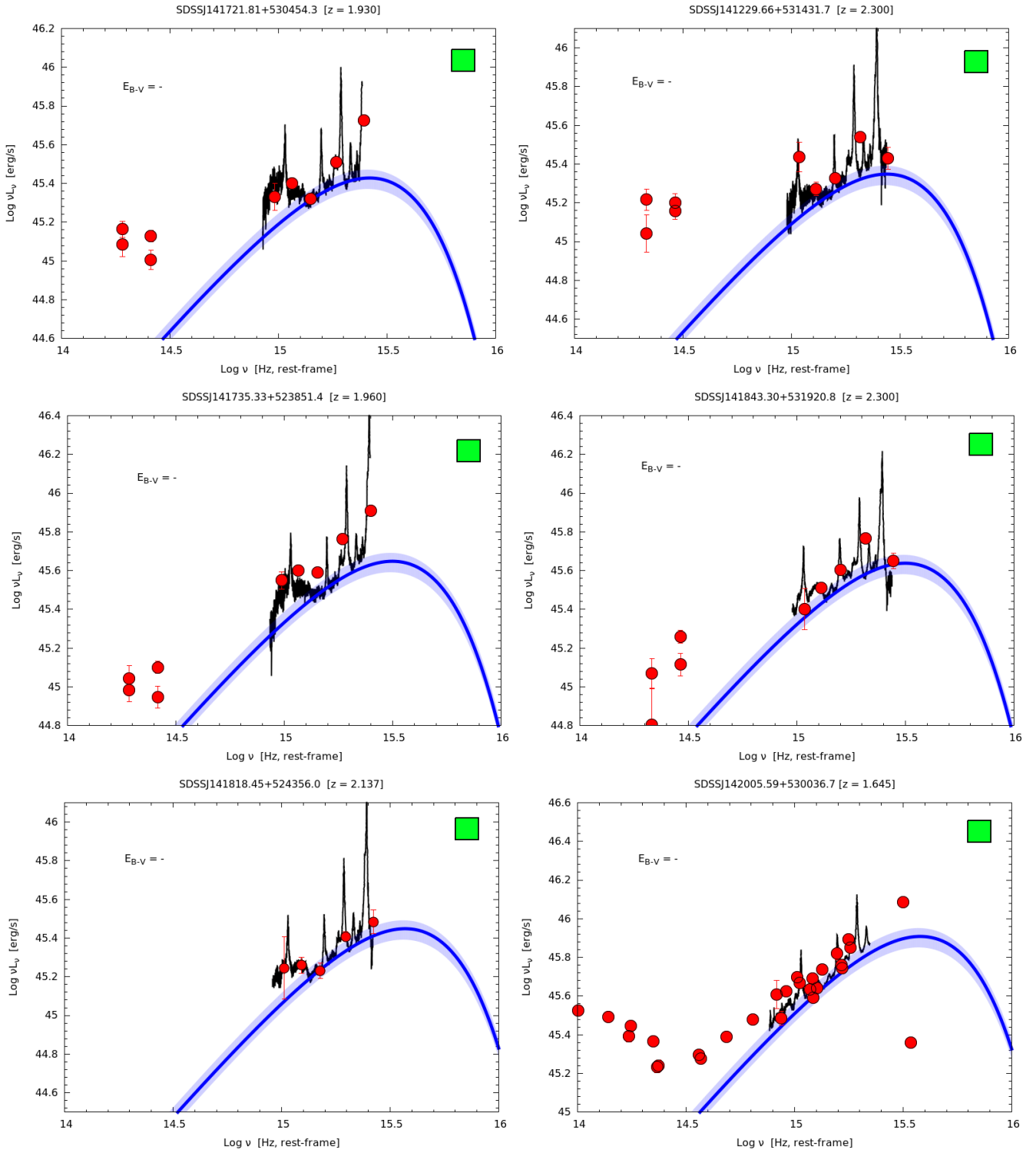


Fig. C.7. continued.

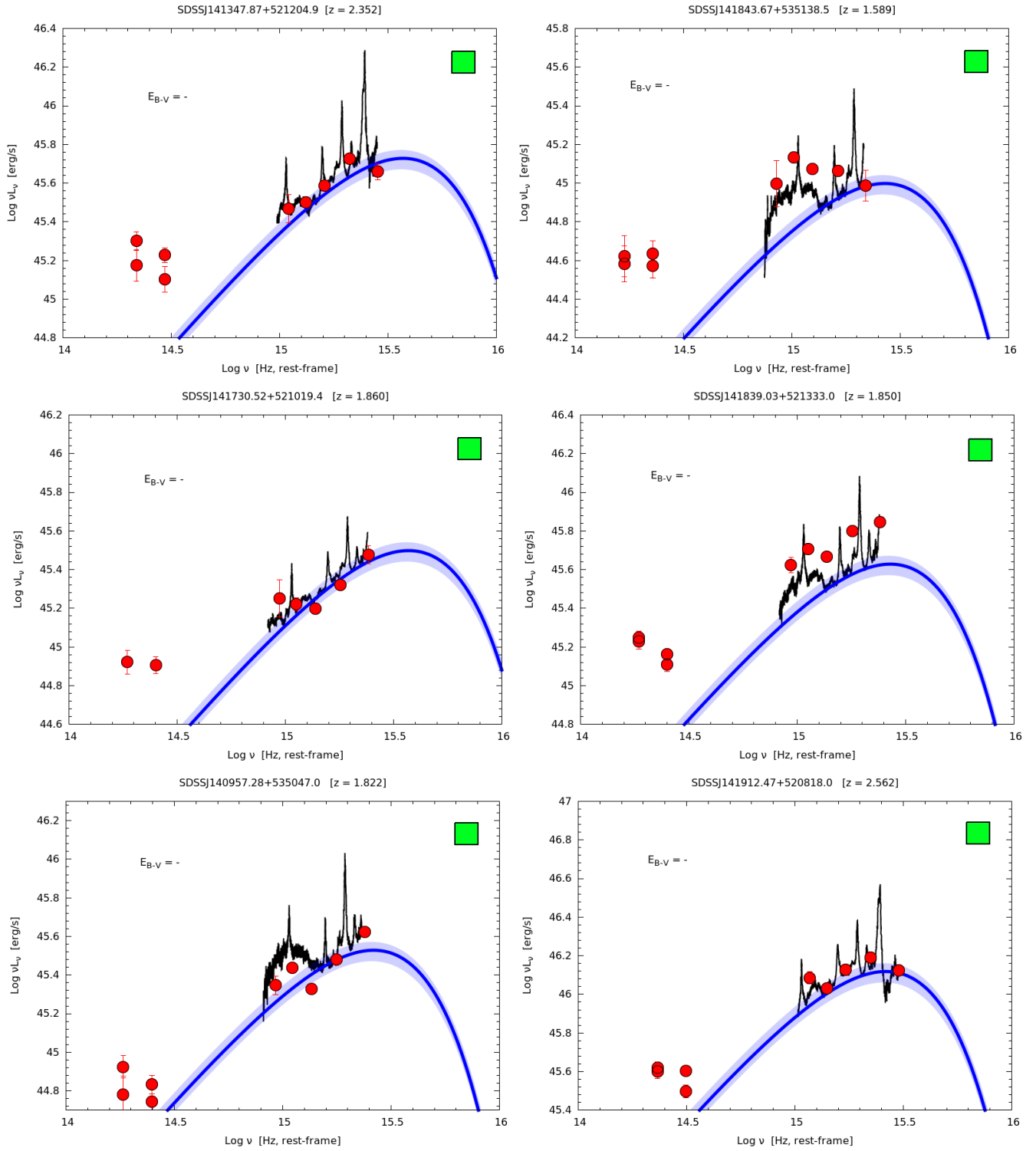


Fig. C.8. continued.

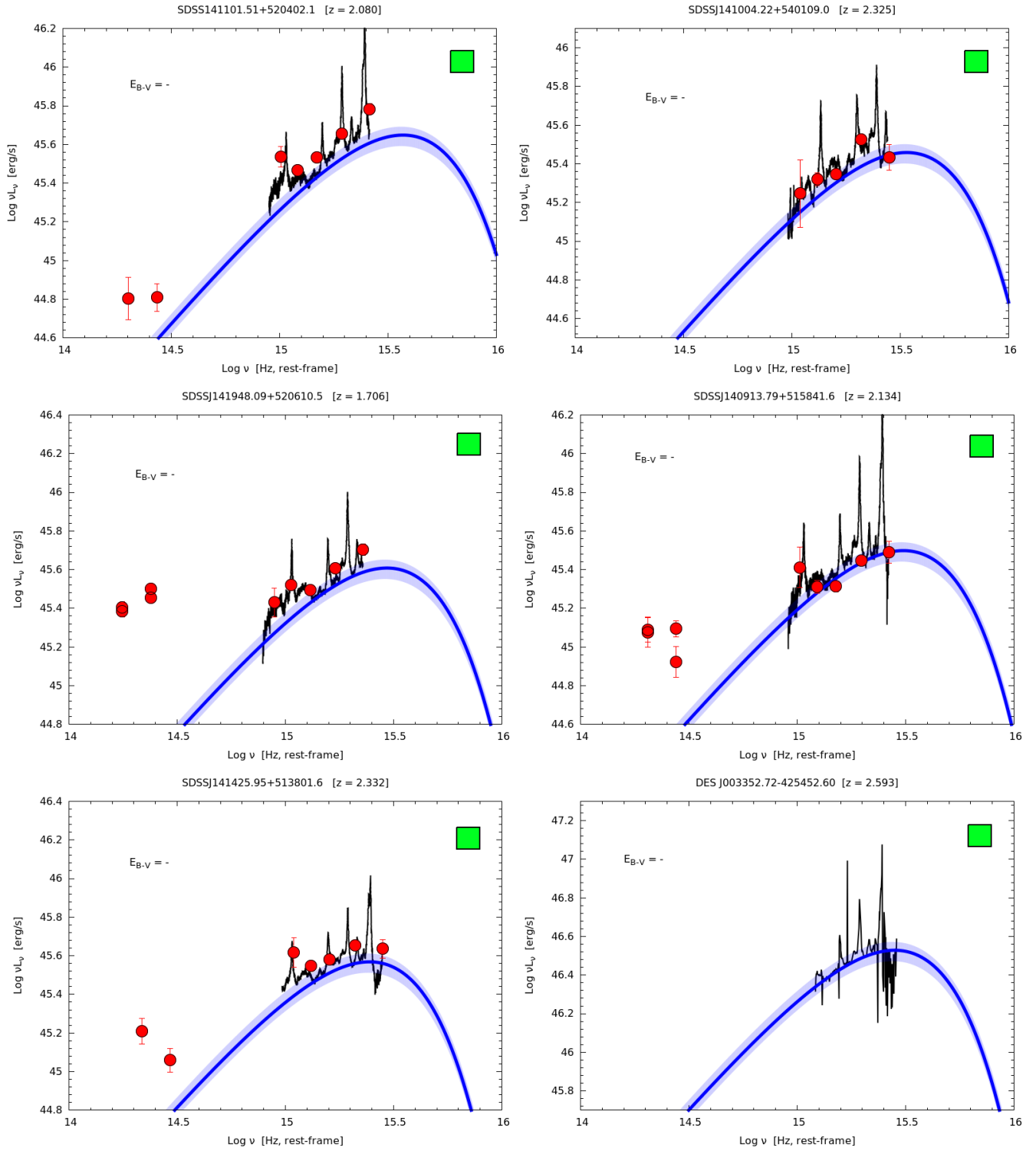


Fig. C.9. continued.

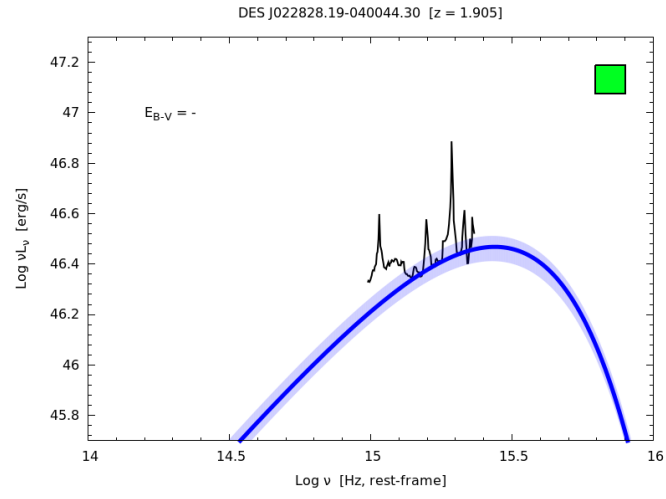


Fig. C.10. continued.

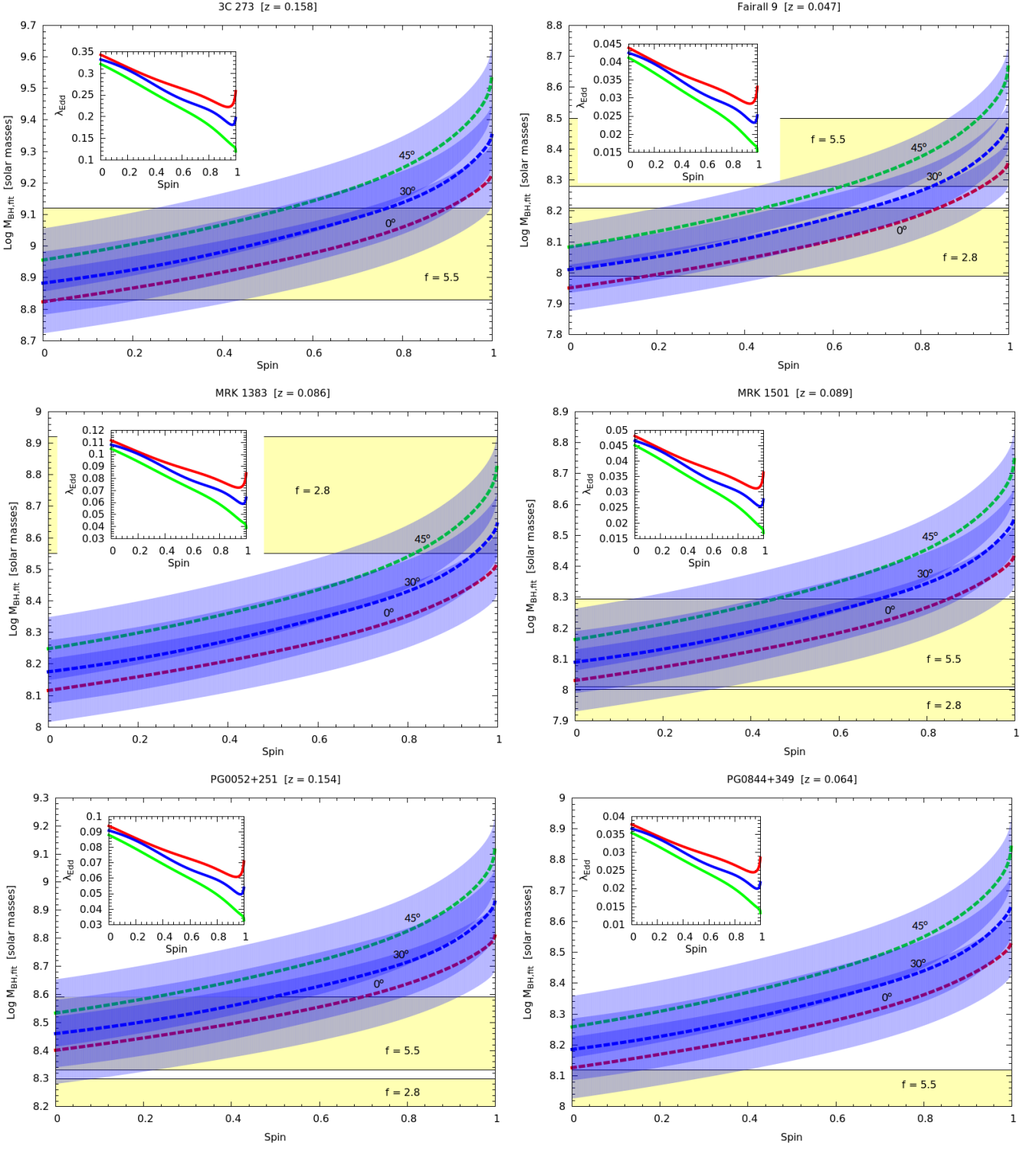


Fig. C.11. KERRBB BH mass as a function of the spin. The dashed red line is the case with viewing angle $\theta_v = 0^\circ$; the dashed blue line is the case with $\theta_v = 30^\circ$; the dashed green line is the case with $\theta_v = 45^\circ$. The shaded blue areas are the confidence intervals obtained after the spectrum fit. The shaded yellow areas are the BH masses from RM with $f = 2.8$ and $f = 5.5$ (the thickness of these areas represents the uncertainty coming from the uncertainty on the light-travel time and the line velocity dispersion): when they are not present, an arrow indicates that the RM estimate is smaller/larger than our estimate. On each plot, the Eddington ratio as a function of the black hole spin is plotted following the same color code adopted for the mass. For the sources MRK142, MRK335, PG1411+442 and SDSSJ141859.75+521809.7, a shaded red area is also present on the plot: it corresponds to the fit performed after the correction of the spectrum from dust absorption for which a large extinction E_{B-V} has been adopted (see Tables A.1 and A.2).

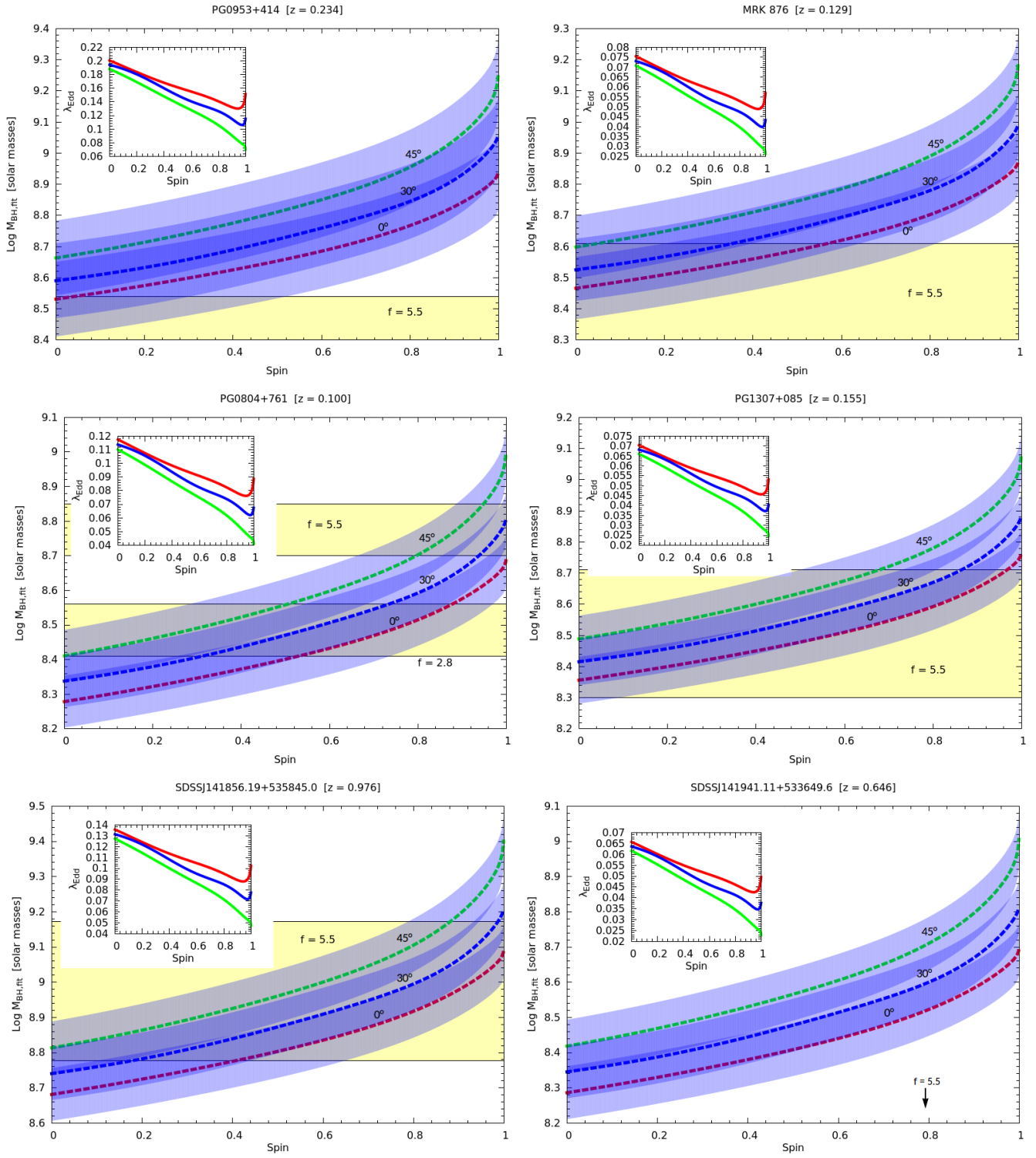


Fig. C.12. continued.

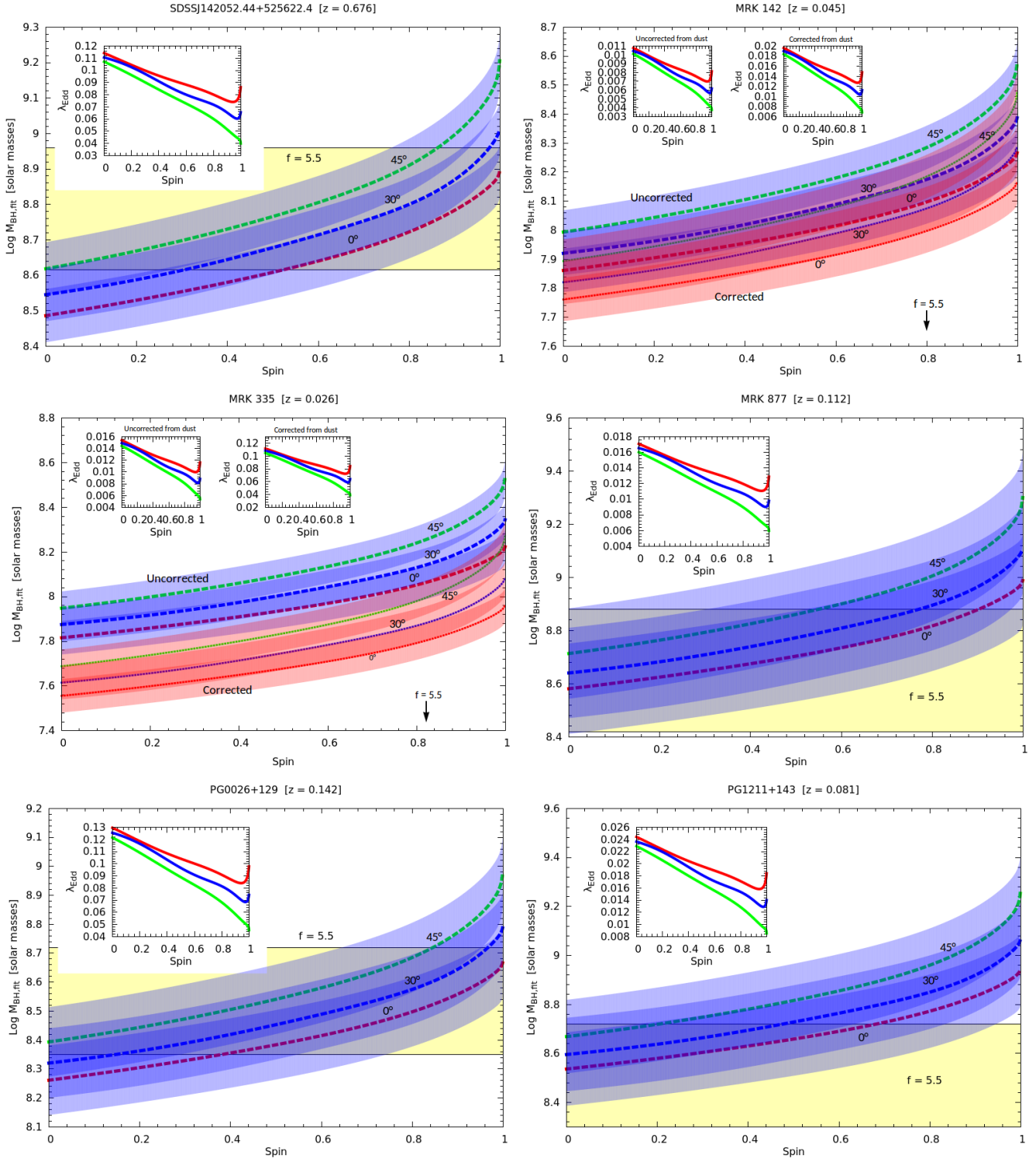


Fig. C.13. continued.

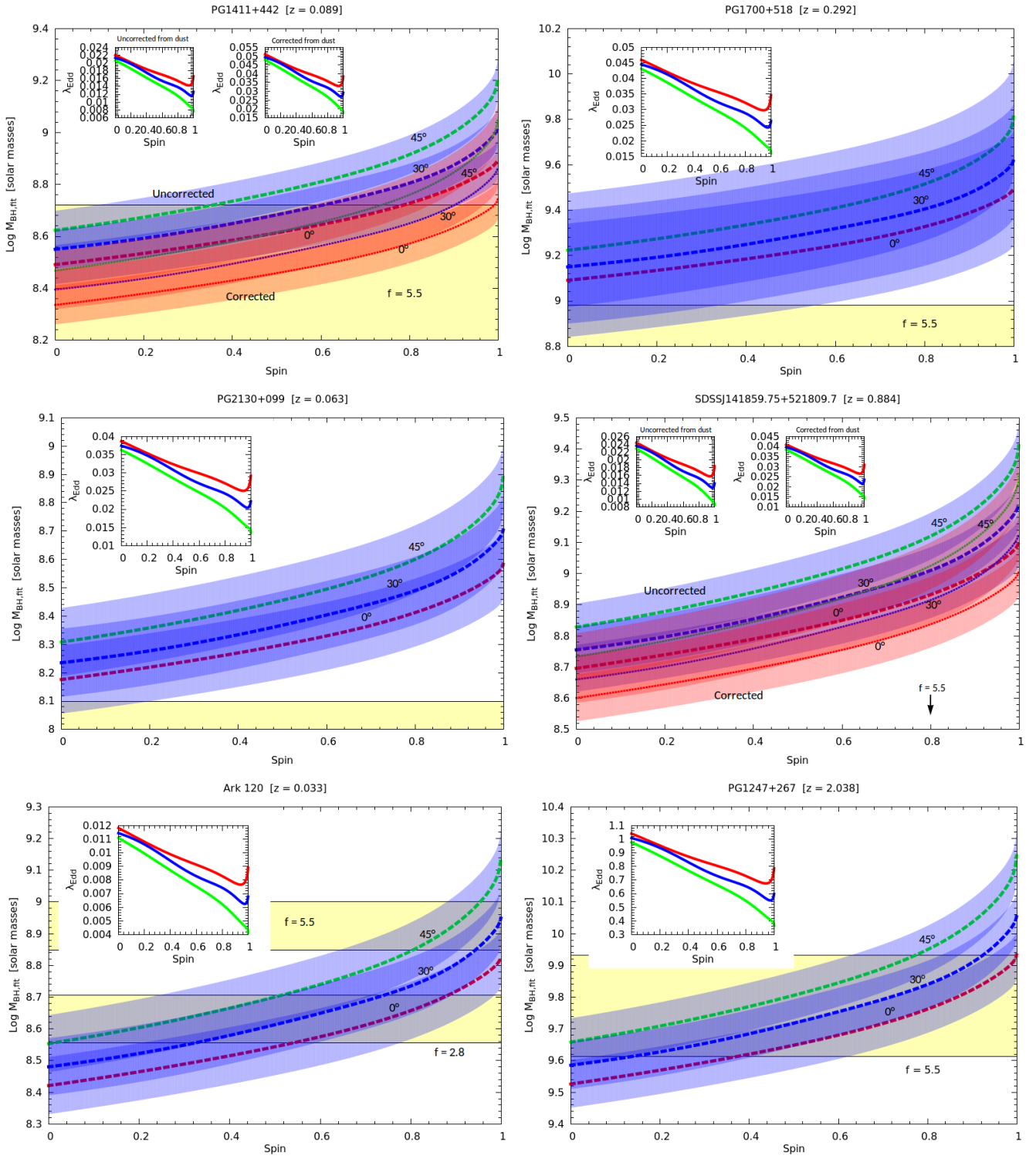


Fig. C.14. continued.

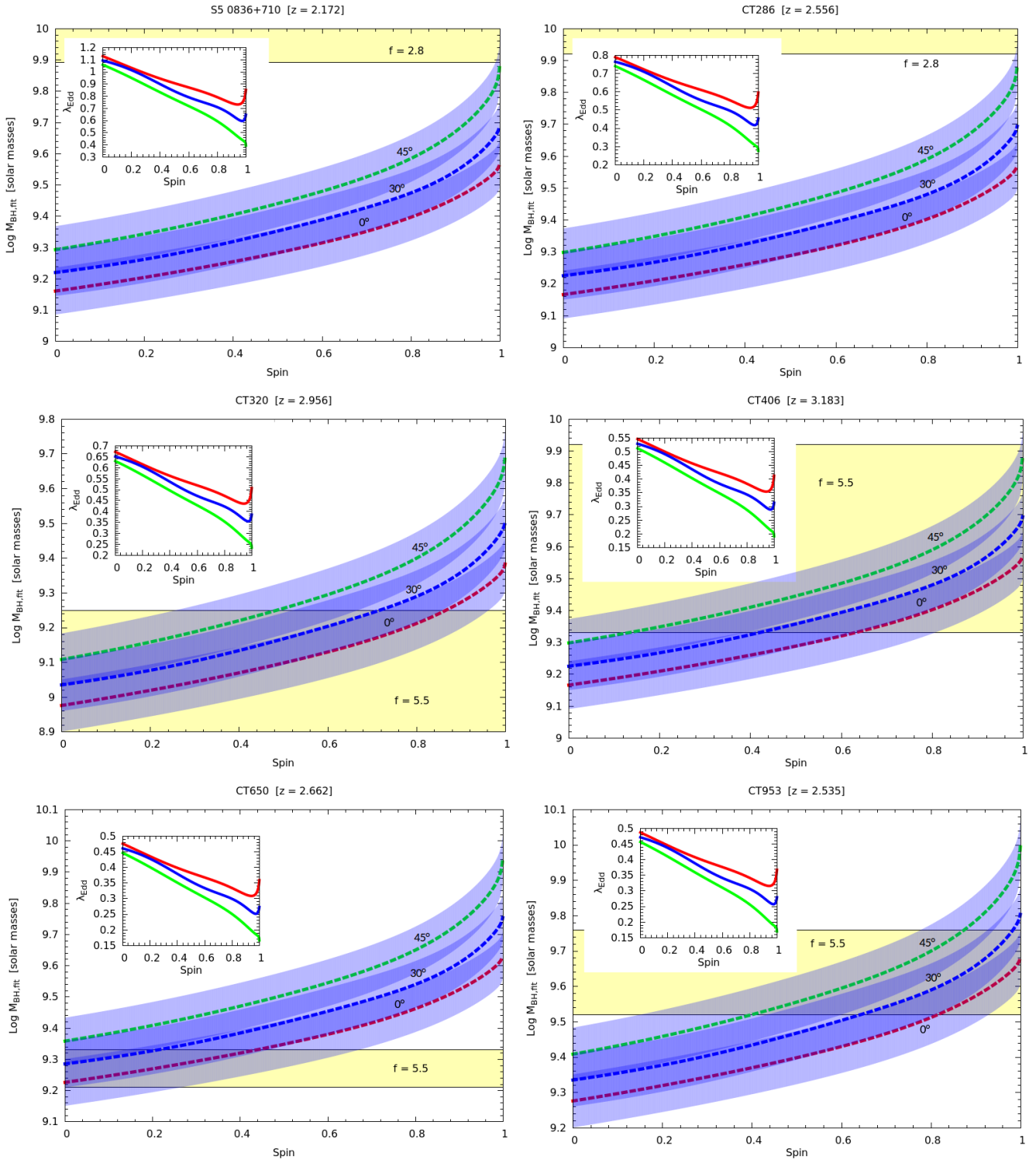


Fig. C.15. continued.

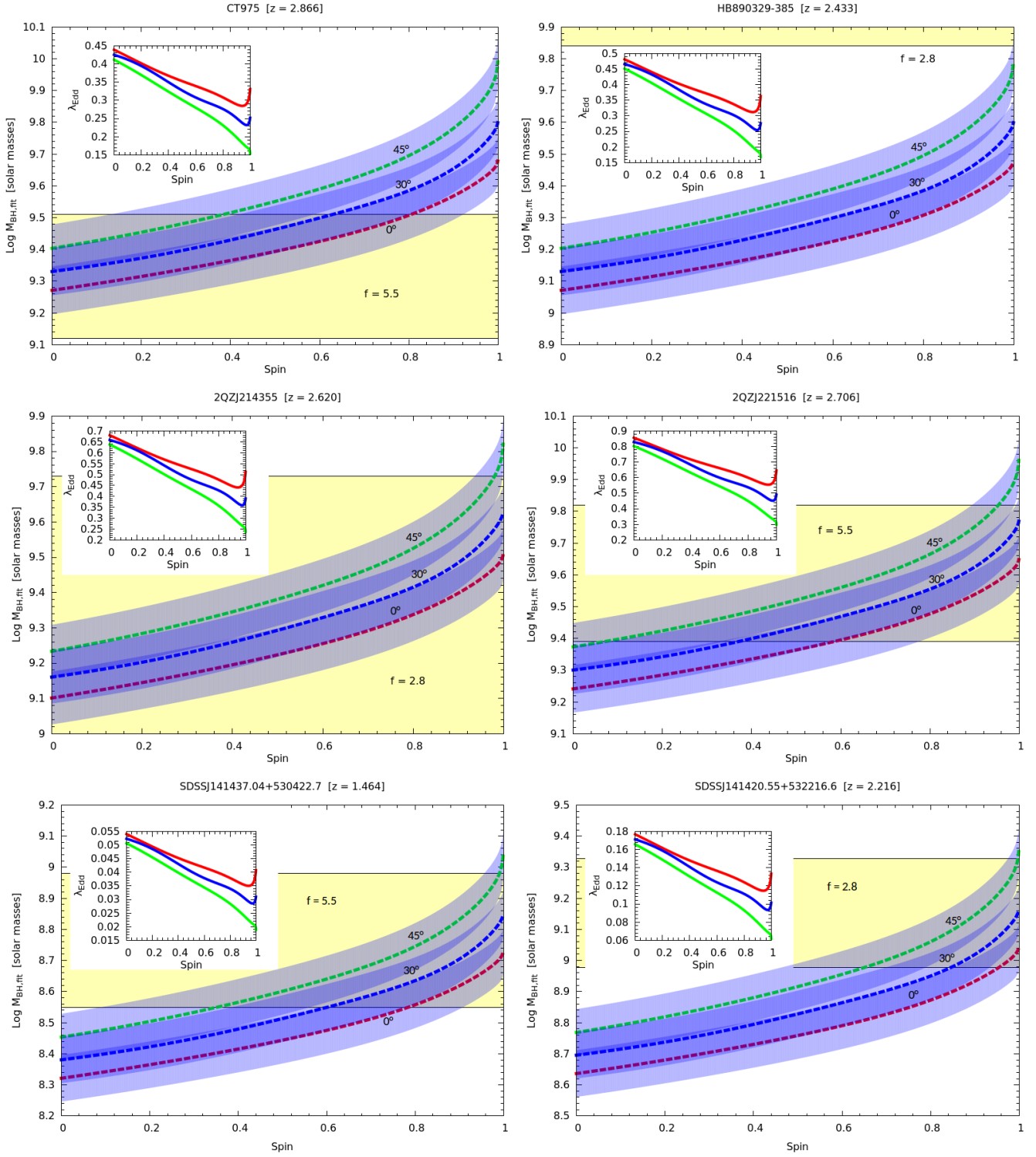


Fig. C.16. continued.

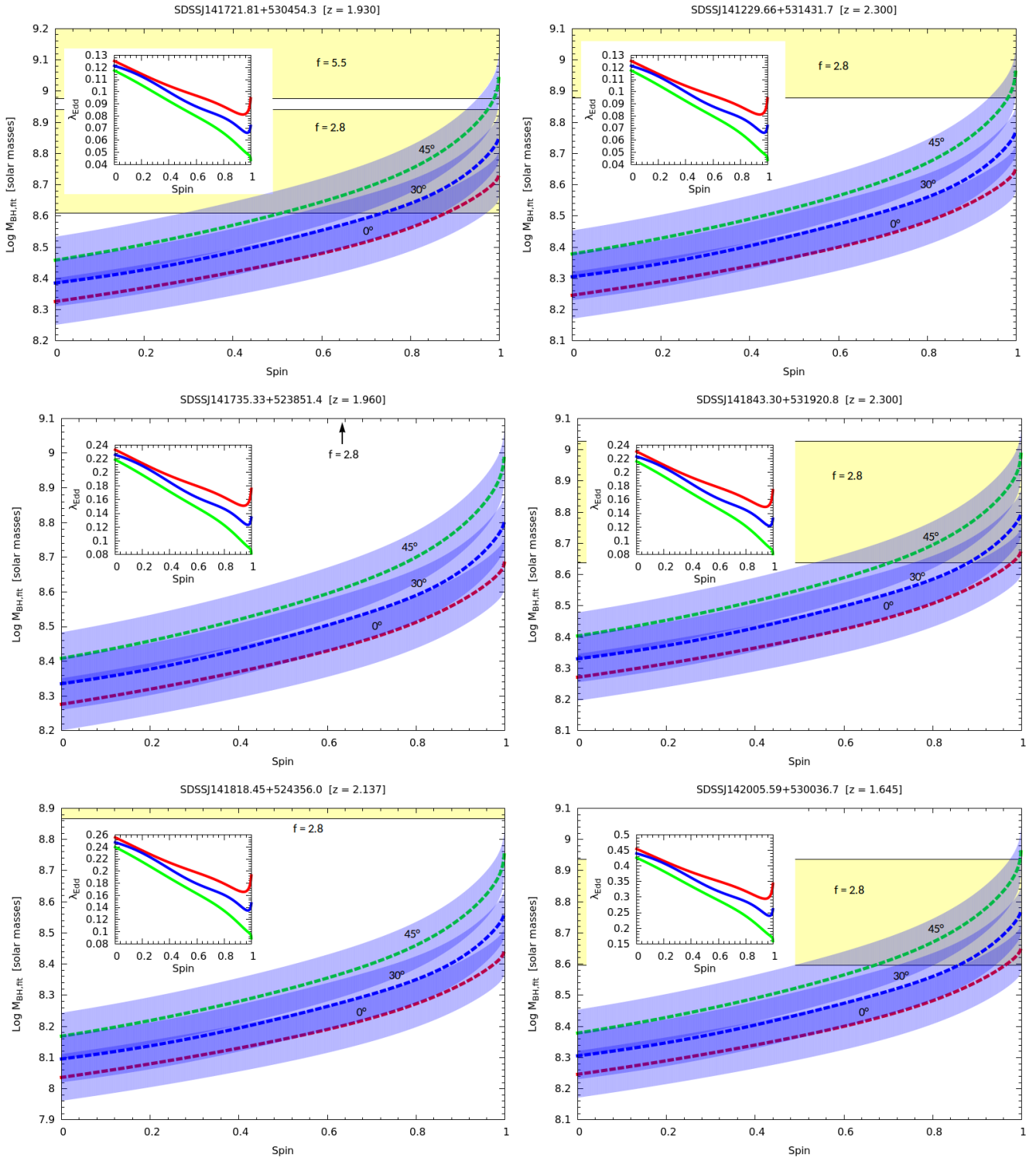


Fig. C.17. continued.

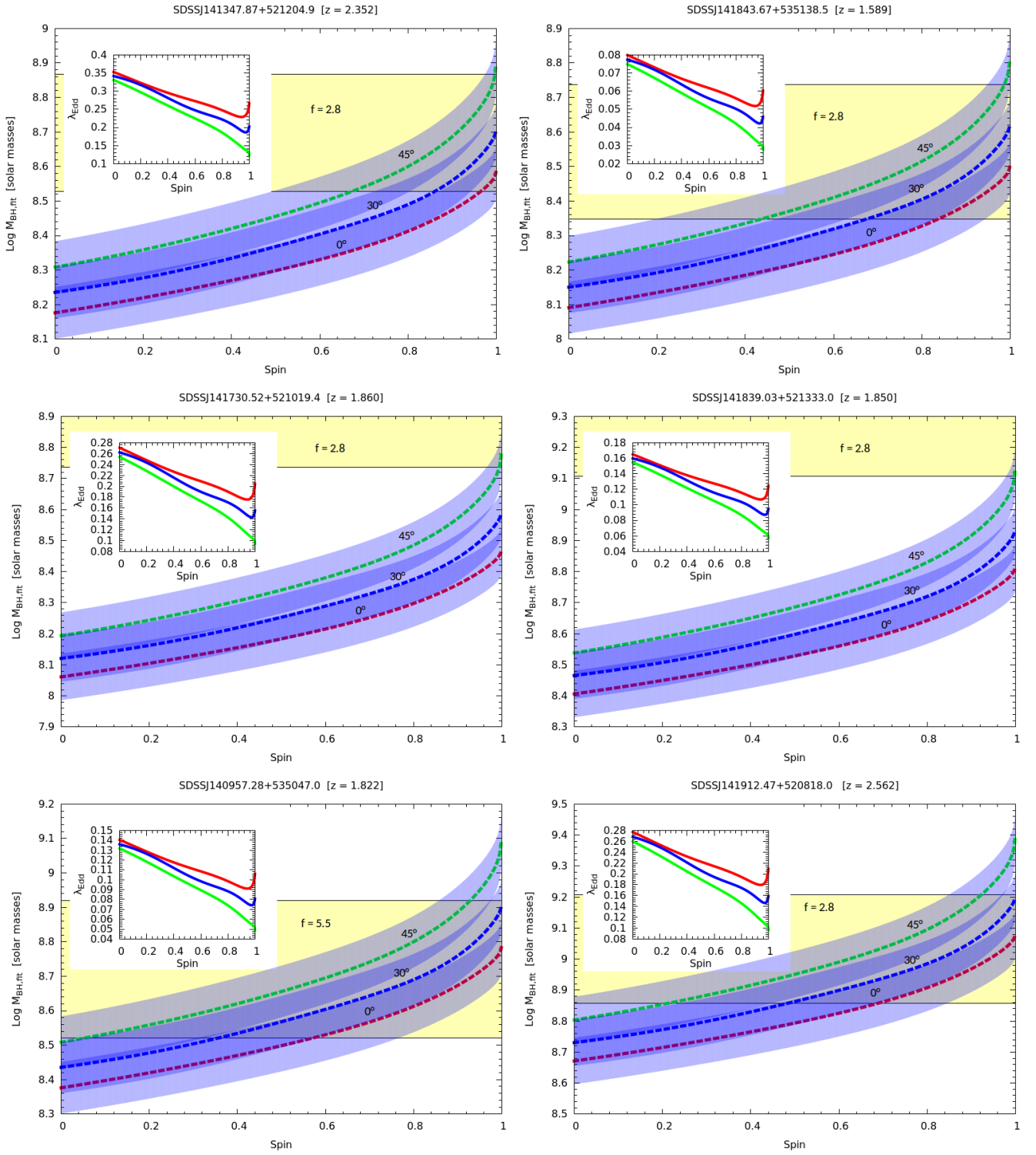


Fig. C.18. continued.

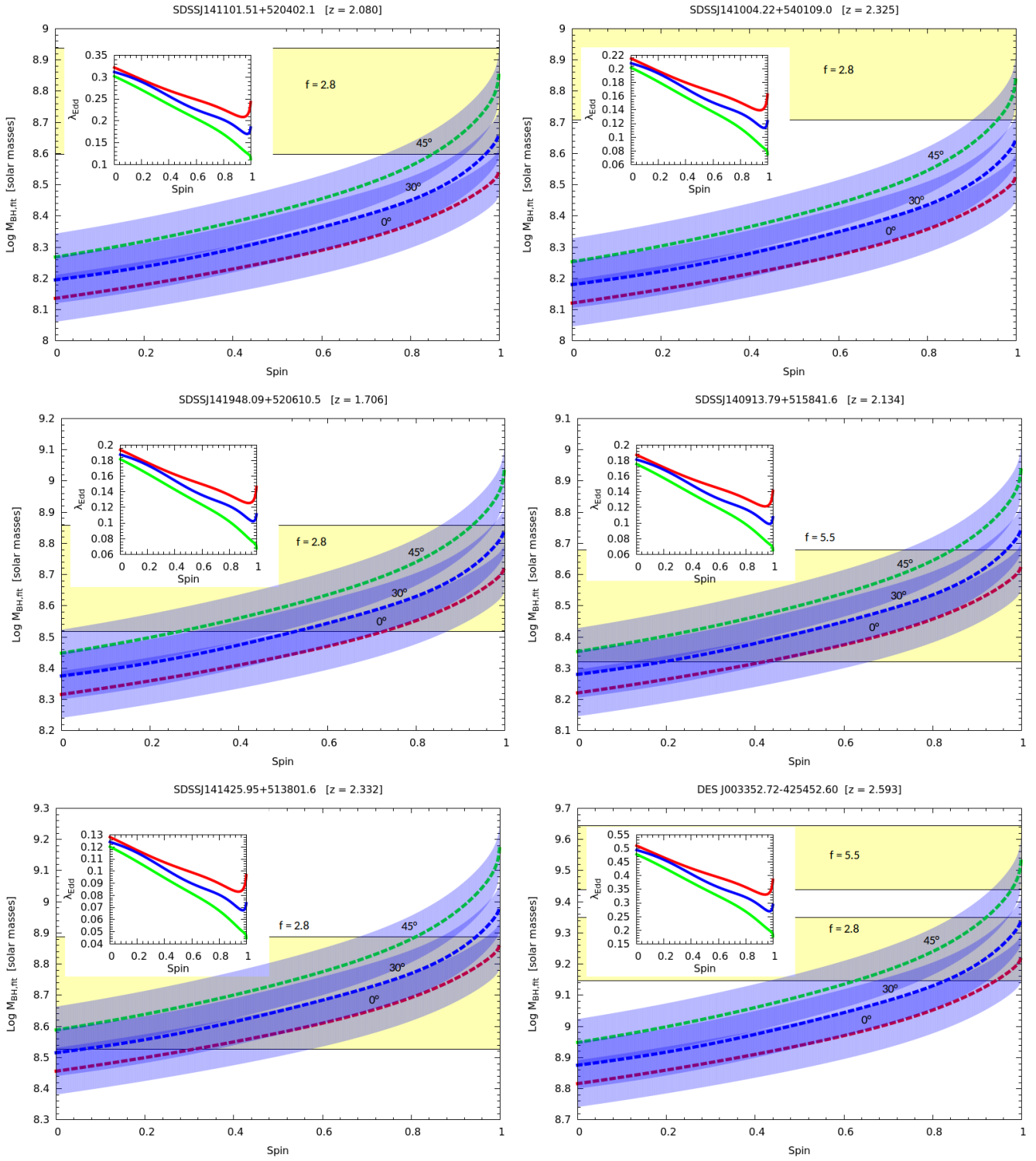


Fig. C.19. continued.

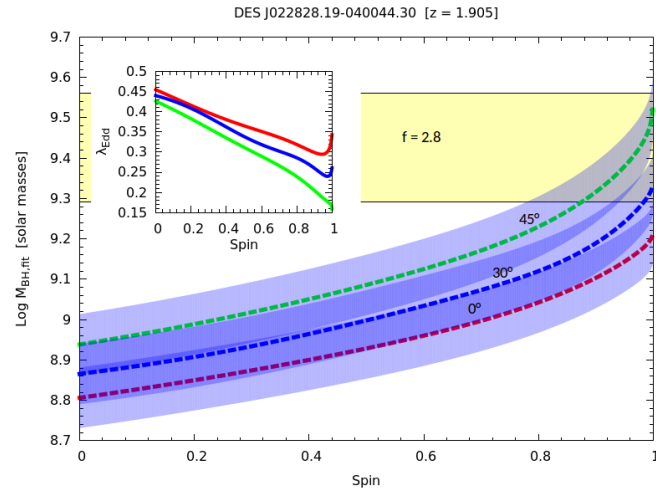


Fig. C.20. continued.